Influence of the bluff body shear layers on the wake of a square prism in a turbulent flow

D. C. Lander, C. W. Letchford, M. Amitay, and G. A. Kopp

Phys. Rev. Fluids **1**, 044406 — Published 9 August 2016

DOI: 10.1103/PhysRevFluids.1.044406

The influence of the bluff body shear layers on the wake of a square prism in a turbulent flow

D.C. Lander and C.W. Letchford
Department of Civil & Environmental Engineering, Rensselaer Polytechnic Institute, Troy, NY, USA

M. Amitay
Center for Flow Physics & Control, Department of Mechanical, Nuclear and Aerospace Engineering, Rensselaer Polytechnic Institute, Troy, NY, USA

G.A. Kopp
Boundary Layer Wind Tunnel Laboratory, University of Western Ontario, London, CA

Despite a substantial body of literature dealing with the effects of freestream turbulence (FST) on $2D$ square cylinders, there remains some open questions regarding the influence of the bluff body shear layer development in a highly perturbed environment and the resulting impact on bluff body flow characteristics. Accordingly, flows with ambient and enhanced FST were studied at $Re_D = 5.0 \times 10^4$ using long duration Time Resolved Particle Image Velocimetry (TR-PIV). The data indicate a narrowing and lengthening of the mean wake and an accompanying rise in base pressure. Using triple decomposition, the underlying dynamics of the wake revealed a streamwise lengthening of the individual von-Kármán (VK) vortex structures, complementing the increase in mean wake length. Close inspection of the shear layer region, in the presence of FST, indicated a substantial increase in curvature towards the body but no pronounced increase in the growth rate. The loci of maximum turbulent kinetic energy and spanwise vorticity in the shear layer region further revealed that the most pronounced changes occurred during the very initial stages follow separation. Inspection of a series of instantaneous PIV fields of *Q-Criterion* showed that the conventional transition pathway, via the formation and subsequent pairing of the Kelvin-Helmholtz (KH) vortices, was bypassed. The KH vortices are observed to immediately cluster and amalgamate before breaking into smaller random eddies. The bypass transition was followed by shear layer reattachment in some cases. This is considered a primary mechanism responsible for the reported changes in the global flow characteristics and the altered wake dynamics. Furthermore, a quantitative definition of the "diffusion-length" was implemented to the square cylinder wake and its relationship with to Strouhal number and wake formation length was considered.

I. NOMENCLATURE

Parameters:
C_{pb} – Coefficient of base pressure
C'_L – Coefficient of fluctuating lift
$\overline{C}_p$ – Coefficient of mean pressure
C'_p – Coefficient of fluctuating pressure
D – Model breadth & depth
d – Diameter of turbulence generating rod
f – Frequency
H – Model spanwise length (z-coordinate)
l – Distance between rod and body
L_D – Diffusion-length
L_F – Wake formation length
Re_D – Reynolds number based on freestream velocity and characteristic dimension of body
U, V, W – Velocity components
$\overline{U}$, $\overline{V}$, $\overline{W}$ – Mean velocity components
u, v, w – Total fluctuating velocity components
$\tilde{u}$, $\tilde{v}$, $\tilde{w}$ – Coherent velocity fluctuations
u', v', w' – Random velocity fluctuations
$\overline{U}_s$ – Velocity outside separation
$\overline{U}_\infty$ – Velocity of freestream
Q – *Q-criterion*
St_D – Strouhal number of VK shedding
$S_\alpha(f)$ – Power spectral density of quantity α
TKE – $2D$-turbulent kinetic energy
y_c – Shear layer position
Γ_0 – Total circulation shed in one cycle of vortex shedding
δ_c – Penetration depth of freestream disturbances
δ_ω – Vorticity thickness of shear layer
ΔC_{pf} – Change in integrated forebody pressure
ΔC_{pb}– Change in integrated afterbody (base) pressure
$\Delta\overline{U}_m$ – Maximum velocity deficit in base region
θ – Momentum thickness of shear layer
ϕ – Phase angle of phase averaged flow field
ω – Vorticity

Abbreviations:
FOV – Field of View
FST – Freestream turbulence
KH – Kelvin-Helmholtz
TR-PIV – Time Resolved Particle Image Velocimetry
VK – von-Kármán

II. INTRODUCTION

The separating shear layers are unambiguously important to the flow characteristics of the bluff body wake. Their presence forms the necessary conditions for the von-Kármán (VK) vortex street, arguably the most distinguishable and notoriously obstinate flow feature in fluid mechanics. As a matter of course, the passage to turbulence in these shear layers, which may be influenced by freestream flow disturbances, necessarily affects the wake dynamics and the loading on the body. As early as 1930 it was known that differing levels of ambient freestream turbulence (FST) would alter parameters such as drag and fluctuating lift circular cylinders [1] and of normally aligned flat-plates [2]. Despite such history, the influence of FST on the bluff body shear layers and the concomitant affects on aerodynamic characteristics such as base pressure, C_{pb}, drag, C_D and wake formation length L_F, have yet to be explicitly and throughly studied.

The importance of the bluff body shear layers is exemplified in the subcritical Reynolds regime ($Re_D \sim 10^2$ to 2×10^5) where vorticity generated at separation is known to be intrinsic to the formation of the von-Kármán vortex street. In fact, in this range, the VK vortex street can form without a wake producing body just by bringing two shear layers of opposite sign within a communicable proximity of one another [3]. Similarly, VK shedding can be suppressed entirely on a bluff body by preventing their interaction with a splitter-plate [4]. The connection between the bluff body shear layers and the overall aerodynamic parameters has also been well documented; for example, the Kelvin-Helmholtz (KH) instability in the shear layers initiate transition which subsequently moves towards separation with increasing Re. This is accompanied by a reduction in base

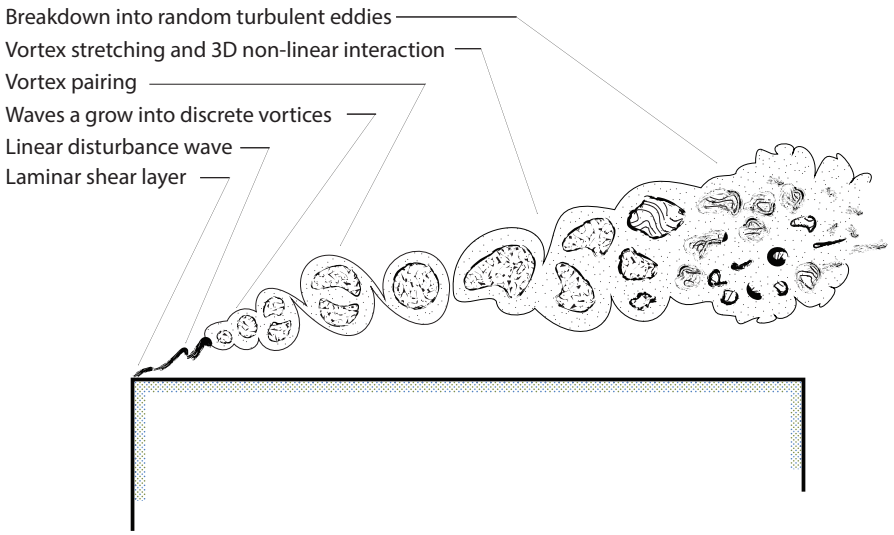

FIG. 1: Physical processes in shear layer transition on square bluff body

pressure C_{pb}, a shrinking of vortex formation length L_F and an increase in the strength of the shed vortices [5]. In particular, there is a lucid connection between the formation length, L_F and the base pressure, C_{pb} as noted by Roshko [6]. This is contingent on the increased Reynolds stresses in the shear layers which increase the turbulent entrainment demand and draw the VK vortices closer to the body; this is accompanied by reduction of base pressure further below the static pressure [6, 7].

It is also well documented that the overall aerodynamic characteristics (C_D, C_{pb}, L_F) are sensitive to the level of FST and some authors have suggested the state of the shear layer contributes to these changes [8–10]. Since these studies, considerable attention has been devoted toward understanding the interactions of FST with bluff body flows [11–13]. For small scales of FST—those which scale with the width of the shear layer—it has been speculated that the FST encourages more vigorous mixing and entrainment into the shear layer and thus increases the growth rate of their width. Entrainment from the recirculation region between the body and the shear layer also promotes curvature toward the body [14]. However, many of these hypotheses have been extrapolated from other flows such as planar mixing layers [15], separation bubbles on blunt-flat-plates [16] or normal-plate-splitter-plate geometries [17] but actual measurements of the $2D$ square cylinder bluff body shear layer under increased FST conditions are conspicuously missing from the literature. A feature which strongly distinguishes the square cylinder from its more popular relative—the circular cylinder—is the presence of an afterbody which has the notable effect of allowing periodic or intermittent reattachment, leading to secondary separation from leeward edges. This results in a straightening of the streamlines at the rear of the body, a rise in C_{pb}, increased L_F and weaker vortex shedding [10].

While the effect of transition and the importance of the KH instability of the bluff body shear layer in the subcritical range has been widely documented [7, 18], its importance in studies considering the effects of FST on bluff bodies has been notably discounted. Authors have contended that for high Reynolds number flows, transition occurs shortly after separation and for this reason that the addition of FST would be unlikely to result in significant changes if the only effect is to promote earlier transition [9]. Hiller & Cherry [19] expressed this neatly while studying the effects of FST on a separation bubble of a blunt-flat-plate: "Stream turbulence may provide a stronger mechanism for shifting the start of transition, but since this appears to occur close to separation anyway it seems more plausible that the main effect is on the subsequent development of the turbulent structure". However, the "turbulent structure" of the bluff body shear layer is itself intrinsically dependent on the passage of turbulence transition, which requires the formation of coherent structures [20–22]. The transition features of the bluff body shear layer are illustrated in Fig. 1 where the laminar KH instability causes the shear layer to roll up and form concentrated centres of vorticity through the receptivity of the laminar separation to small disturbances. These structures grow and maintain integrity downstream of separation (similar to planar-mixing layers) as they entrain fluid and diffuse vorticity; the initial process scales with the momentum thickness and accordingly it is Reynolds number dependent with the ratio of the shear layer frequency f_{KH} to the von-Kármán frequency, f_{VK} changing according to $f_{KH}/f_{VK} \propto Re^n$, where $n = 0.67$ for circular cylinders [23] and $n = 0.70$ for square cylinders [21]. The coherent shear layer vortices pair (possibly more than once) via a non-linear mechanism and the associated large deformations in the vorticity distributions subsequently cause a breakdown into random turbulent eddies [24].

The effects of FST on bluff body shear layer transition has recently been considered for a circular cylinder [25]; the authors observed that increasing the turbulence intensity brought the location where the breakdown into random turbulent eddies in shear layers occurred closer to separation. They also reported that FST suppressed KH vortex pairing, detected by subharmonic spectral content in a hotwire signal. The description provided therein echoes the altered processes of boundary layer transition during "bypass-transition". Bypass-transition has received considerable attention from the Boundary Layers community in the past two decades [26, 27] and the process is known to be contingent on the development of turbulent spots, which evolve in the presence of streamwise streaks (large instantaneous streamwise velocity fluctuations). Streamwise streaks form in the laminar boundary layer upstream of separation in association with "shear-sheltering", whereby the effects of viscosity prevent

the penetration of high frequency fluctuations into boundary layer but permits strong low frequency disturbances [24]. The bypass-transition is an accelerated transition process which in boundary layers is known to cause skip the initial Tollmien-Schlichting instability. Similarly, these processes have been demonstrated in a shear layer of a separation bubble causing the KH instability to be circumvented and the final stages of transition ensue closer to separation [24, 28]. To date there are no studies which have examined this phenomenon explicitly on the development of a shear layer separating from a bluff body. In the case of a square cylinder aligned normal to the flow, it is known that a large favourable pressure gradient keeps the boundary layer on the front face laminar at very large Reynolds numbers [29]; presumably shear-sheltering effects would also increase and the basic conditions for an equivalent bypass-transition may be prevented. The literature is mute on whether FST creates conditions necessary for a bypass-transition in the bluff body shear layer and to on whether the mechanism of streak formation are indeed necessary for this geometry. Notwithstanding, it is contended here that changes to the transitional structures of the shear layer by the presence of FST, as outlined in Fig. 1 which would constitute variations from a "standard" pathway to a random turbulent state will affect the flow characteristics of bluff body.

Finally, the shear layer plays a role in the phenomenological theory of vortex shedding proposed by Gerrard [30]. In this model, the bluff body shear layer was given its own length scale and coined the "diffusion-length", L_D and notionally defined as the width of the shear layer when freestream irrotational fluid is pulled across the wake centreline by the action of the opposite VK vortex. It was introduced as an artefact to balance the decreasing formation length, L_F, with increasing Reynolds number on a circular cylinder in the presence of the remarkably stable non-dimensional shedding frequency, St_D across the subcritical range. The opposing tendencies of L_F and L_D are thought to act via the same mechanism, namely, the intensity of the turbulence stresses in the shear layer which affect the balance of entrainment rates into the shear layer and forming VK vortex. The entrainment rates into the shear layer are also known to be sensitive to FST, and thus so to is the vortex formation process in Gerrard's theory. However, while L_F has been studied in depth, attempts to quantify L_D are missing from the literature, except for the work of Norberg [31] who observed a complex interplay between L_F, L_D and St_D on a circular cylinder in the presence of flows with added FST. This is perhaps due to the difficulties of obtaining reliable measurements in the turbulent formation region of the bluff body. Furthermore, the use of a parameter such as L_D has not been considered on the square cylinder geometry, where the shear layer is known to be affected by the presence of the afterbody. In particular, with added FST, it is known that formation length, L_F increases rather than decreases, as in the case of the circular cylinder. Thus a further goal of the current study is to make an estimate of L_D and consider its utility on the square cylinder geometry in relation to St_D and L_F.

In Summary, the purpose of this paper is to study the contribution of the shear layer separating from a $2D$ square cylinder under the effects of freestream turbulence. In particular, to explore how turbulent fluctuations affect shear layer development and how these impact basic flow/aerodynamic characteristics such as drag, base pressure and wake formation length is the goal. It is intended to substantiate the mechanisms frequently cited in the FST-bluff body literature such as increased growth rates and curvature of the shear layer, intermittent reattachment and altered transition processes and relate them to the above aerodynamic parameters. Accordingly, the paper is structured as follows: § III presents the details of the experiment and measurement systems; § IV describes the analytical treatment of the PIV data used to obtain a triple decomposition of the flow field; § V presents the findings of the study, first considering gross parameters such as drag obtainable from the pressure measurements. A comprehensive analysis of the base and wake follows with a detailed investigation of the changes attributable to the coherent and random fluctuations in the base and wake. The shear layer region is then closely considered in order to understand the origins of the observed downstream changes. In § VI the implications of these findings are discussed and in § VII conclusions are presented.

III. EXPERIMENTAL METHOD

A. Model & facilities

The experiments were performed in the sectional-model/bridge-deck test section of the closed-loop Tunnel II at the Boundary Layer Wind Tunnel Laboratory (BLWTL) at the University of Western Ontario. A square cross-section model of $D = 76.2$ mm and length aspect ratio of $H = 10D$ was assembled of unpolished extruded aluminium, as shown in Fig. 2. The model was mounted horizontally at the tunnel centre on a rig between endplates. The rig was placed approximately 4 m downstream of the tunnel contraction where the cross-sectional dimensions measured 1.83 m high by 3.34 m wide. The blockage ratio based on the tunnel height and the model width (between endplates) was 4.2%; corrections were made to the drag coefficient, C_D and base pressures C_{pb} using the theoretical formulations of Maskell [32].

B. Flow conditions

The Reynolds number was $Re_D = 5.0 \times 10^4$ based on a mean tunnel velocity of $\overline{U}_\infty = 10$ m/s. A clear signature of vortex shedding was present at the $St_D = fD/\overline{U}_\infty = 0.132$ ($f \simeq 17Hz$). A small increase in mean streamwise velocity of $\simeq 2\%$ was observed at a local Pitot-static tube placed between the endplates, as compared to the upstream reference Pitot. The ambient FST in the tunnel was 1%.

A turbulence generating 'rod' of diameter $d/D = 0.104$ was placed $l/D = 4.69$ ($l/d = 45$) diameters upstream of the body

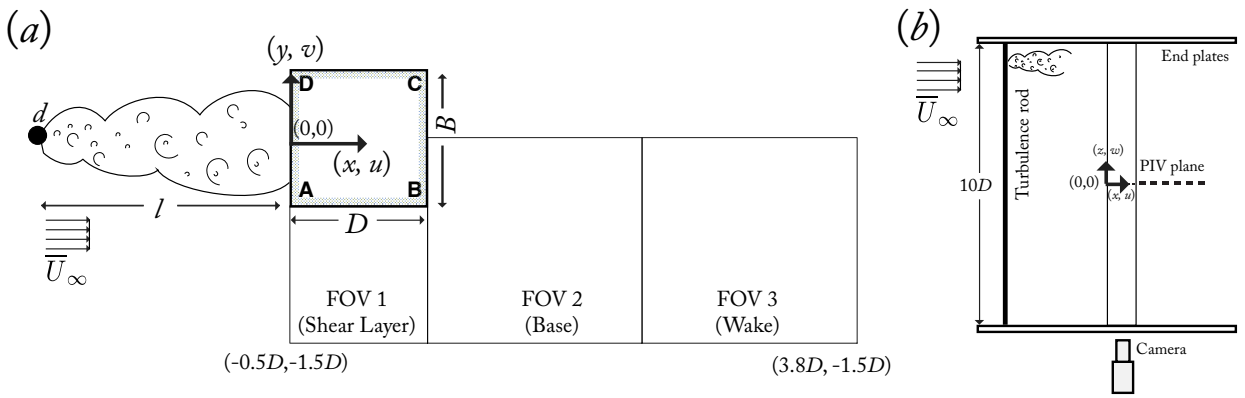

FIG. 2: (a) model arrangements along the centreline of the sectional model, illustrating the relative position of the turbulence generating rod and square cylinder. Three FOV show the TR-PIV measurement domain taken in the lower half of the wake; (b) plan view of model illustrating camera position and PIV measurement plane.

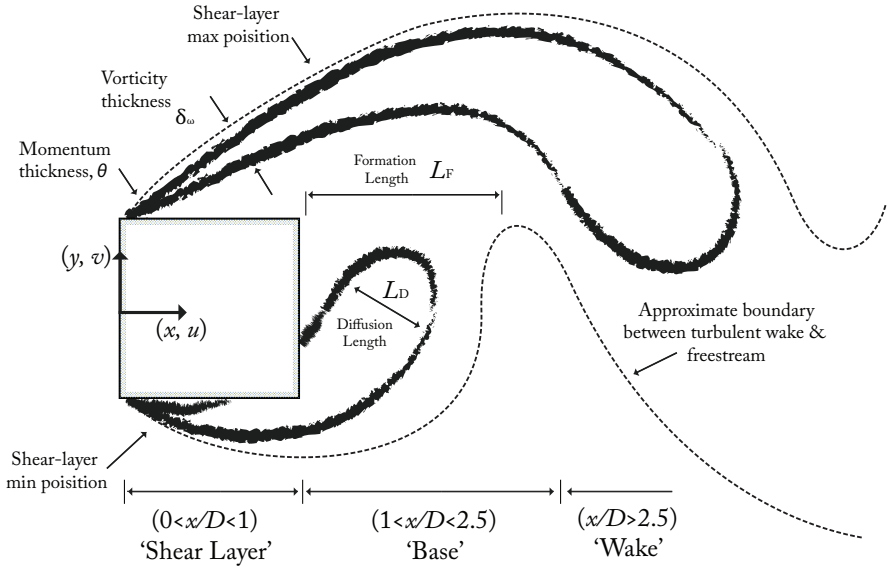

FIG. 3: Dimensions & length scales of the flow domain

along the stagnation streamline, as shown in experimental setup, Fig. 2 and summarised in Table I. It is noteworthy that the magnitude of velocity taken outside of separation, $\overline{U}_s$, at $(x/D,\, y/D) = (0.05,\, 0.61)$ directly contributes to the total circulation shed into the wake [33]. Here, the normalised total circulation shed during a single cycle is $\Gamma_0/\overline{U}_\infty D = 1/St(\overline{U}_s/\overline{U}_\infty)^2$, and importantly, between cases, there is only an 8% reduction of total circulation with the addition of FST by this estimation. In Fig. 3 some characteristic flow parameters and dimensions are illustrated. The mean velocity deficit based on the total velocity and the turbulence intensity in the longitudinal direction are shown in Fig. 4. In addition, Fig. 4 (a) also displays Eq. 1, the similarity solution of a turbulent wake computed for the turbulence generating cylinder [34]. Qualitatively, the wake of the rod fits the theory well. Hotwire measurements were made on the wake centreline of a circular cylinder at $x/d = 35$ at $Re_d = 5764$. It was noted under these conditions, the spectral content was broadband and contained no signatures of vortex shedding at $St_d = 0.21\%$. Rather, it neatly matched the von-Kármán spectrum, including the $-5/3^{rd}$ decay, based on a the determined integral length scale.

$$\frac{\Delta\overline{U}}{\Delta\overline{U}_m} = e^{\left(\frac{y}{0.0256\sqrt{xd}}\right)^2} \tag{1}$$

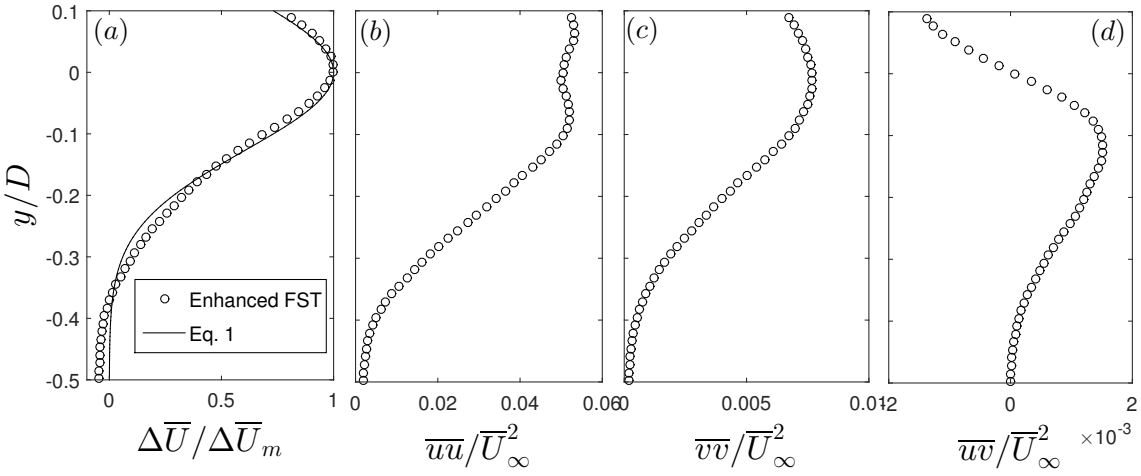

FIG. 4: cross-stream profiles in the wake of the turbulence generating rod. All data are longitudinal flow components at $x/D = -1.3$ with the model present: (a) mean velocity deficit. Also graphed is the wake profile given by Eqn. 1 for a similarity profile of turbulent wake where, $\Delta\overline{U} = \overline{U}_\infty - \overline{U}(y)$ is the velocity deficit and $\Delta\overline{U}_m = \overline{U}_\infty - \overline{U}(y)_{min}$ is the largest deficit at the wake centreline; [34] (b) streamwise normal Reynolds stress; (c) cross-stream normal Reynolds stress; (d) Reynolds shear stress

TABLE I: Flow conditions

Test	Case	d/D	l/D	l/d	Re_d	$\Delta\overline{U}_m$	$\sqrt{\overline{uu}}/\overline{U}_\infty$	L_u^x/D	$\overline{U}_s$	$\Gamma_0/\overline{U}_\infty D$
Ambient FST	A	-	-	-	-	-	1.0%	-	$1.40\overline{U}_\infty$	7.42
Enhanced FST	B	0.10	4.69	45	0.53×10^4	$0.86\overline{U}_\infty$	6.5%	0.33	$1.34\overline{U}_\infty$	6.80
Gartshore [9]	-	0.08	3.25	39	0.33×10^4	-	6.8%	< 1	-	-

C. Measurements

Velocity measurements in the lower half of the cylinder wake and unsteady surface pressure measurements around the complete circumference were acquired. Pressures were acquired at a sampling frequency of 1108 Hz for 80 s resulting in 88640 points/channel for each test; simultaneously, TR-PIV data were obtained at 1000 Hz (image pairs at 500 Hz) for 50 s resulting in 25000 vector fields for each field of view.

1. Unsteady Pressures

Surface pressure measurements were made on the circumference of the square cylinder at centre span ($z = 0$), with 48 total taps (12/face), as illustrated in Fig. 2 (b). Pressure measurements weren't A 762 mm tube system connected the 12.7 mm surface mounted hypodermic taps to a 16 channel high speed differential pressure scanner. The tube system comprised two PVC segments of 305 mm and 330 mm, attaching to the model and scanner respectively. The PVC tubes were joined by two brass restrictors in series which created a system with a flat frequency response up to 200 Hz and linear phase over the same range. The reference pressure was the static pressure from the Pitot-static tube while each channel was normalised by the reference dynamic pressure obtained from a Pitot-static tube placed approximately 2 m upstream of the model.

2. Particle Image Velocimetry

As shown in Fig. 2 (a), PIV data were obtain for three Field of View (FOV), nominally corresponding to the regions of the shear layer, base, and wake in the lower half of the square cylinder. The data were acquired using the long duration, time-resolved system developed at UWO [35]. Whereas most TR-PIV systems employ RAM storage, this system is remarkably

capable of streaming and storing large quantities of data through the use of a set of fibre-channel hard-drive arrays (IO Industries Inc.). Images were acquired at a sampling rate of 1000 Hz using a single Photron FASTCAM PCI CMOS camera with 17 μm square pixels, 1024×1024 pixel resolution and a 10-bit ADC sensor. This resulted in vector fields resolved at 500 Hz with a spatial range of $1.6D \times 1.6D$, see Fig. 2 (a). Seeding particles were atomised olive oil with a mean particle diameter of 1 μm while illumination was provided by a double head, diode pumped, Nd:YLF (527 μm) Darwin-Duo laser by Quantronix which provided 22 mJ/pulse per frame. Cross-correlation of the images was performed using a multi-pass setting of a single-pass 64×64 pixel interrogation window with 50 % overlap followed by a dual-pass 32×32 pixel interrogation window with 75% overlap. Post processing smoothed the data in order to eliminate specious vectors, resulting in vector fields contained 128×128 vectors with ~ 1 vector/mm^2.

IV. ANALYTICAL TREATMENT

A. Triple decomposition

The flow around a square cylinder features large-scale quasi-coherent motions with strong periodicity of von-Kármán vortex structures. With this feature, it is convenient and insightful to decompose the flow into contributions from organised and random motion. Following the notation of Hussain & Reynolds [36], a flow variable, for example the streamwise velocity, U, can be separated according to Eq. 2

$$U = \overline{U} + u = \overline{U} + \tilde{u} + u' \tag{2}$$

Where $\overline{U}$ is the time invariant mean, u is the total fluctuating component which can be separated into $\tilde{u}$, the contribution of the organised motion and u', the random turbulent fluctuations. Because $\tilde{u}$ is a zero-mean cyclical process intrinsic to the flow, phase locking the time resolved data provides a subset of vector fields with constant phase. More formally, data are organised into constant phase sets $\phi = 0, 1, 2...31$ and the ensemble average of the subset of N_ϕ vector fields is taken:

$$\langle U \rangle^\phi = \frac{1}{N_\phi} \sum_{n=0}^{N_\phi} U_n \qquad (\phi = 0, 1, 2...31) \tag{3}$$

For the current experiment with large-scale coherent vortex shedding at $f \simeq 17$ Hz, a typical cycle was sampled 29.4 times by the time resolved PIV system. The PIV images were conditioned for acceptable variation in amplitude and frequency prior to sorting into constant phase sets. The start of a phase cycle was identified as a peak in pressure signal at the tap on the upper face nearest separation; this signal was first low pass filtered at 25 Hz to remove high frequency fluctuations not associated with VK vortex shedding. The data were then sorted into 32 discrete phase subsets with each containing approximately $N_\phi \simeq 900$ before the phase averaged statistics were determined. The unsteady pressure signal was sampled simultaneously during each acquisition of the three FOVs, however, as the pressure and PIV acquisitions were not synchronised, the vector fields were re-sampled by linear interpolation to their nearest pressure neighbour (in time) such that the PIV and the pressure signals were synchronous.

The data sampled at constant phase include both the mean and the contributions from the coherent motions, $\langle U \rangle^\phi = \overline{U} + \tilde{u}^\phi$. It follows that the contribution of the coherent motion at some phase ϕ can be isolated removing the time invariant mean: $\tilde{u}^\phi = \langle U \rangle^\phi - \overline{U}$. The contributions to the turbulent stresses can also be elucidated; for example, the global shear stresses are decomposed: $\overline{uv} = \overline{\tilde{u}\tilde{v}} + \overline{u'v'}$. Similarly, the Reynolds shear stresses at constant phase are decomposed $uv^\phi = \tilde{u}\tilde{v}^\phi + \langle u'v' \rangle^\phi$. Cantwell & Coles [37], highlighted properties of this decomposition which are worth re-echoing: the time-mean of the coherent motions over a cycle is zero, $\overline{\tilde{u}} = 0$; the average of random fluctuations at constant phase is zero, $\langle u' \rangle^\phi = 0$ and the periodic and random motions are uncorrelated, $\overline{\tilde{u}u'} = 0$.

V. RESULTS

A. Pressure Analysis

In this section, the results of the experiment described in § III are presented. There are two experimental cases discussed in great detail, namely, 'Case A' (ambient FST) and 'Case B' (enhanced FST). In § V A an analysis of the unsteady pressure data are used to calculate global time-averaged loads such as C_{pb} and C_D. This is followed by comprehensive analysis of the flow field in the base and wake in § V B which also considers changes separately attributable to the coherent and random fluctuations. In § V C the shear layer region is closely analysed in order to understand the origins of the observed changes in the wake.

The mean and fluctuating pressure distributions are presented in Fig. 5 (a) & (b), respectively, for both cases along with the normalised spectra of drag (c) and lift (d). In addition, the results of Bearman & Obasaju [38] are presented for ambient FST ($\sqrt{\overline{uu}}/\overline{U}_\infty < 0.04\%$) flow in frames ($a$) and ($b$). Good agreement is observed in both cases with slight exception on the leeward face where lower magnitude C'_p values were recorded. On the windward face for Case A, $\overline{C}_p = 1$ at stagnation while it is slightly reduced in the FST case due to the momentum deficit of the turbulence generating rod. On the leeward face, the

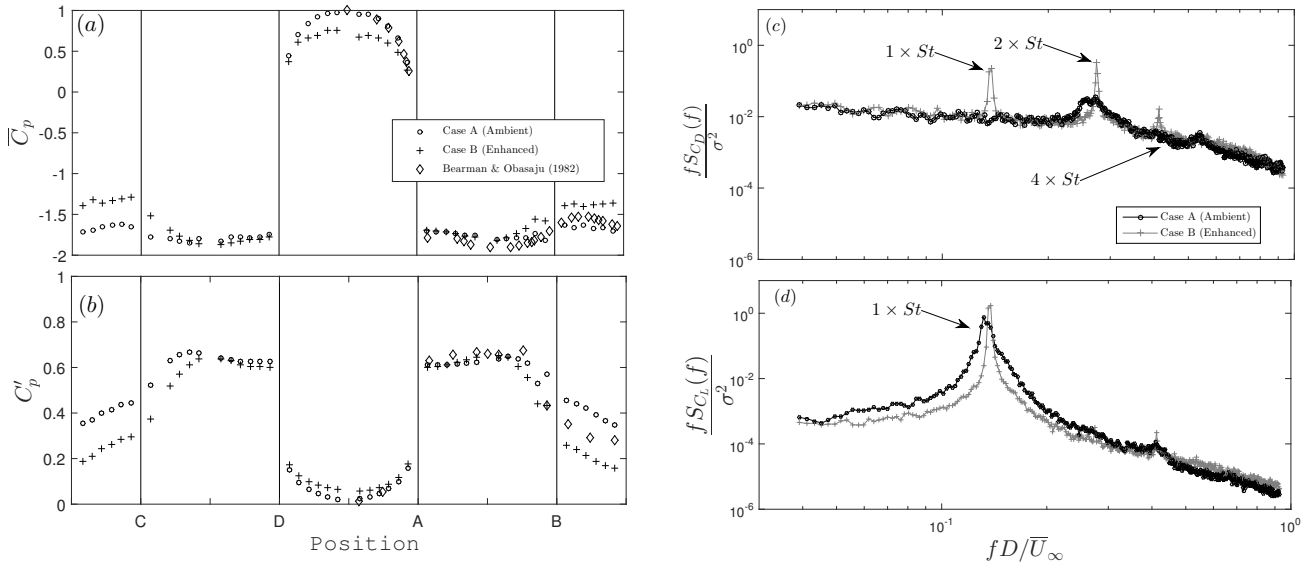

FIG. 5: (a) mean pressure coefficients; (b) fluctuating pressure coefficient; (c) spectrum of drag; (d) spectrum of lift.

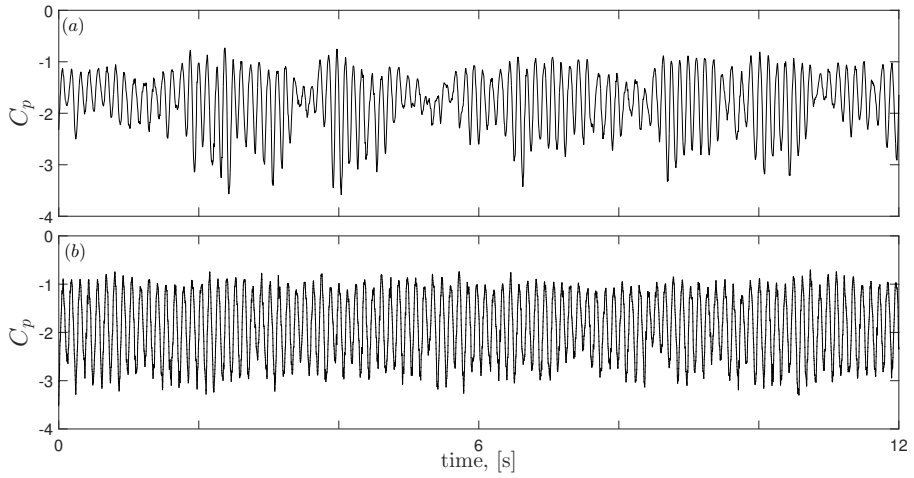

FIG. 6: time history of pressure coefficients (a) Case A; (b) Case B

mean pressure coefficients are less negative for Case B. With ambient FST, C'_p values are significantly larger near the trailing edges and in the wake than the enhanced FST case, consistent with Lee [39].

Fig. 5 (c) & (d) display the normalised spectra of drag and lift, respectively. As expected, in (c) the spectral peak at $2 \cdot St_D$ is due to the streamwise influence of each VK vortex; however, in the enhanced FST case, peaks are also clearly observable at $1 \cdot St_D$ & $4 \cdot St_D$. In (d) the dominance of the VK vortex shedding is evident, and curiously, in a similar manner to the spectra of drag, the enhanced FST case exhibits a narrower range of frequencies with larger amplitude that are associated with the VK vortex shedding. Additionally, the shedding frequency for the enhanced FST case is slightly higher with $1.05 \times St_{(CaseA)} \simeq St_{(CaseB)}$. For a $2D$ square, Nakamura & Ohya [13] also witnessed a concentrating of the spectral content of the streamwise velocity in the near wake with enhanced FST turbulence ($\sqrt{\overline{uu}}/\overline{U}_\infty = 10.8\%$, $L^x_u/D = 0.32$). In Fig. 6 a comparison of the pressure time history at a tap on the lower face at $x/D = 0.5$ is presented. In frame (a), Case A evidently displays larger variation, with an apparent low frequency modulation of the pressure peaks. This phenomenon was discussed by Roshko [6] and reported by Szepessy & Bearman [40] who associated it with a "spanwise modulation of the vortex shedding phase" which was likely caused by extrinsic end effects. In the presence of enhanced FST, the spanwise modulation is mostly absent, indicating the $3D$ effect is disrupted. This has an organising effect and is likely responsible for the concentrating of the spectral energy around $1 \cdot St_D$ as well as at the emergence of harmonic peaks. In Fig. 7, the correlation coefficient of the the lift at several normalised spanwise

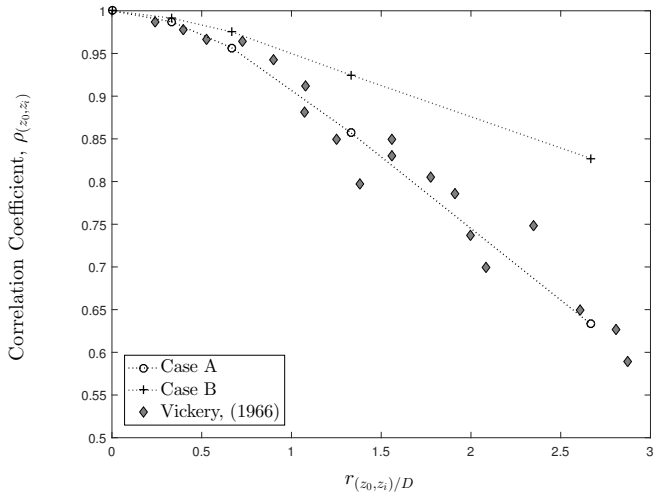

FIG. 7: Correlation coefficient, ρ, calculated on the fluctuating lift, C'_L across the model span. $\rho_{(z_0,z_i)}$ is a measure of the linear dependence between the fluctuating lift calculated over the normalised spanwise distance, $r_{(z_0,z_i)/D}$

TABLE II: Mean and fluctuating forces

Study/case	$\sqrt{\overline{uu}}/\overline{U}_\infty$	C_D	ΔC_D	$-C_{pb}$	C_{pf}	$-\Delta C_{pb}/\Delta C_D$	$\Delta C_{pf}/\Delta C_D$	C'_D	C'_L
Current (Case A)	1.0%	2.35	-	1.51	0.84	-	-	0.22	1.14
Gartshore [9]	0.6%	2.22	-	1.44	0.77	-	-	-	-
Bearman & Obasaju [38]	0.04%	2.29	-	1.57	0.72	-	-	-	-
Current (Case B)	6.5%	1.86	0.49	1.22	0.61	0.59	0.41	0.15	1.10
Gartshore [9]	6.8%	1.68	0.54	1.05	0.63	0.72	0.28	-	-

distances, $r_{(z_0,z_i)/D}$, is presented along with the similar data of [41], where fair agreement is observed with the comparable conditions. Here it is noted that for Case B the flow is more correlated over the range of observed locations. This is analogous to a disruption in the spanwise modulation of the vortex shedding phase hypothesised by [40].

Table II compares the mean drag and base pressure calculated by numerically integrating the pressure distributions (with some relevant literature); also reported are the forebody and afterbody contributions to the pressure drag. The quantities in Table II have been normalised by the length between outer most pressure tap locations, $0.84D$, as no pressure data was available near the corners. The drag in the current case is slightly higher than that of Gartshore [9], but within 3% of that reported by Bearman & Obasaju [38].

The changes to the drag coefficients attributable to the introduction of a momentum deficit by the turbulence generating rod must be distinguished from those of the altered aerodynamics, to which this paper is concerned. This is considered as the proportion of the change in drag between cases, ΔC_D, attributable to the forebody, $\Delta C_{pf}/\Delta C_D$, and base, $-\Delta C_{pb}/\Delta C_D$. For the current study, 59% of the drag reduction is caused by changes in base pressure which result from changes to the flow field. Gartshore [9] reported approximately 72% of the drag reduction was caused by the changes to the base pressure, but also noted while testing rods of different diameters ($d/D = 0.08$ & $d/D = 0.17$) that the drag did not change considerably by increasing the rod size if the turbulence intensity was equivalent. This suggests that there is weak coupling between the imposed momentum deficit and the aerodynamics of the wake.

Comparing force data for square cylinders with similar, grid generated flow fields helps contextualise and validate the reach of the findings. The widely cited work of Lee [39], for grid generated turbulence ($\sqrt{\overline{uu}}/\overline{U}_\infty = 4.5\%$, $L^x_u/D = 0.59$) reported a change in base-pressure of 17.6%; for Petty [42] ($\sqrt{\overline{uu}}/\overline{U}_\infty = 5.4\%$, $L^x_u/D = 0.76$) it was 14.0%, while for the present study, this reduction was 19.2%. Thus excluding the forebody influence, the rod has comparable effects on the base-pressure and presumably, the altered aerodynamics of the formation region. With this in mind, the authors contend that the method employed by Gartshore [9] demonstrates considerable merit and warrants further investigation.

Also included in Table II are the fluctuating body forces, C'_D and C'_L. It is noted that in both cases, the fluctuating forces on Case B are below Case A. This agrees with the distributions of C'_p presented in Fig. 5(b). The reductions in C'_D are entirely attributable to the pressures on the base (actually, C'_p increases on the front face); this is consistent with the findings of Bearman & Obasaju [38] and likely due to an increase in the formation length of the wake. This point will receive further attention in § V B. The changes in C'_L are less pronounced, although agree with the findings of Gartshore [43] who observed the fluctuating lift declining in a similar manner to the base-pressure and drag with increasing turbulence intensity.

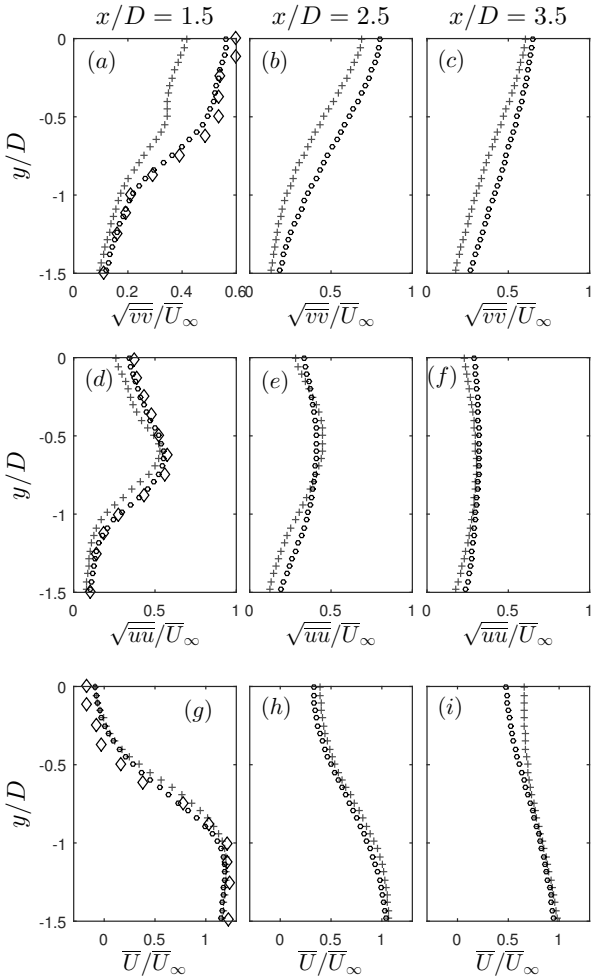

FIG. 8: Cross-stream distributions of $(a-c)$ r.m.s of cross-stream velocity, $(d-f)$ r.m.s of streamwise velocity; and $(g-i)$ mean streamwise velocity; $\circ$, Case A, present; $+$, Case B, present; $\diamond$, ambient FST ($\sqrt{\overline{uu}}/\overline{U}_\infty \simeq 2\%$), Lyn *et al.* [44].

B. The base & wake regions

1. *Base & wake regions: Mean flow*

Figs. 8 & 9 present the mean streamwise velocity and r.m.s profiles at three x/D locations and along the centreline respectively. For the case with ambient FST, the results of Lyn *et al.* [44] are also presented and good agreement is observed between the related data throughout the base and wake regions. The vortex formation length, L_F, defined as the distance along the wake centreline from the origin to the location of maximum $\sqrt{\overline{vv}}/\overline{U}_\infty$ can be estimated from Fig. 9 (a) as $L_{F(A)} = 2.21$ and $L_{F(B)} = 2.46$ while for Lyn *et al.* [44], $L_{F(Lyn)} = 2.37$.

Fig. 10 presents time-averaged streamlines originating near the upstream corners, (a) Case A and (b) Case B. As can be seen, with enhanced FST, the base region has narrowed and elongated slightly while the recirculation regions under the shear layers are reduced in size. Gartshore [9], hypothesised the addition of FST of sufficient intensity would increase the curvature of the shear layer and cause it to reattach to the body near the leeward corners. The shear layer must subsequently re-separate from the leeward edge, resulting in a straightening of the streamlines in the streamwise direction. These characteristics are consistent with the current results shown in Fig. 10.

These mean flow results and the accompanying pressure analysis show clearly that many of the previously reported effects of FST on the global aerodynamic properties of the $2D$ square cylinder are observed in the current data. The data are consistent

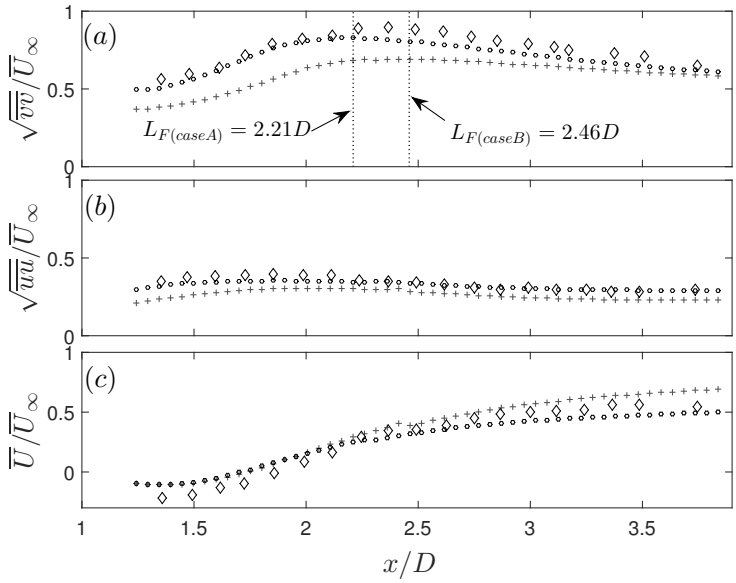

FIG. 9: Centreline wake profiles of (a) r.m.s of cross-stream velocity, (b) r.m.s of streamwise velocity, and (c) mean streamwise velocity; ∘, Case A, present; +, Case B, present; ⋄, ambient FST ($\sqrt{\overline{uu}}/\overline{U}_\infty \simeq 2\%$), Lyn *et al.* [44].

with the literature, where available, and it is apparent that the most distinguishable effects of FST occur within the base region where the VK vortex formation process takes place. However, the altered dynamics, which lead to the afore mentioned changes, are not recoverable from the data presented so far; thus, in the following section, the phase-averaged flow fields in the base and wake regions are presented and discussed. This will provide a better understanding of the role of the shear layer in this process and specifically addressed in § V C.

2. Coherent fluctuations in the base & wake region

The coherent quantities extracted from the triple decomposition outlined in § IV A afford an exploration of the dynamics underpinning the changed global properties presented above. In Fig. 11, the normalised phase averaged vorticity, $\langle\omega_z\rangle^\phi = \overline{\omega}_z + \tilde{\omega}_z^\phi$ over half a shedding cycle ($\phi = 0$ to π) is presented. Recall, similar to Cantwell & Coles [37] and Lyn *et al.* [44], symmetry in the flow domain is exploited to minimise measurement redundancy. Data obtained on the lower wake is reflected about the wake centreline and shifted by π, allowing the full wake to be represented from only the half-wake TR-PIV measurements.

At $\phi = 0$, due to the large scale flapping of the shear layer by the VK vortex formation process, the shear layer on the lower side is near its minimum distance from the side face, observed in (a) & (f); concurrently, the upper shear layer has reached its maximum distance away from the body. Fluid from the base is drawn into the recirculation region beneath the upper shear layer and reverse flow separates from the downstream edge in phases $\phi = \pi/4$ to $3\pi/4$. Phase $\phi = 0$ corresponds to that which was described by Bloor & Gerrard [45], where the action of the growing vortex in the upper half draws the irrotational freestream across the wake centreline from the lower side. The distance from the body where this occurs corresponds to the formation length and is characterised by the largest intensity cross-stream fluctuation on the wake centreline as described by Bloor & Gerrard [45]: "the intensity of the fluctuations on the axis depends on the vortex strength, the position and size of the vortex ... all these factors contribute to the appearance of a maximum [$\sqrt{\overline{vv}}/\overline{U}_\infty$] at the end of the formation region." In Fig. 11 ($a - f$), the formation lengths estimated from Fig. 9 as the location of maximum $\sqrt{\overline{vv}}/\overline{U}_\infty$ on the centreline are also plotted and it is seen to neatly correspond to the downstream edge of the lower forming vortex (still connected to the shear layer) measured by the vorticity in both flow cases. Clearly, the description of Bloor & Gerrard [45] is indeed meaningful and the estimation of L_F from Fig. 9 allows interpretation of the changes to the formation process between cases.

The dynamics accompanying the increased formation length are qualitatively illuminated in Fig. 11: the vortices are elliptically transformed and elongated in the streamwise direction. This result complements observations made of the steady wake streamline of Fig. 10, whereby the enhanced FST increases the length and decreases the width of the wake. However, as observed in Fig. 9, the wake lengthening is also associated with a substantial reduction in the cross-stream fluctuations, $\sqrt{\overline{vv}}/\overline{U}_\infty$. Clearly, the ability for cross-stream communication between shear layers is affected; this is notionally consistent with the secondary reattachment and streamline straightening argument forwarded by Gartshore [9]. This point will be further

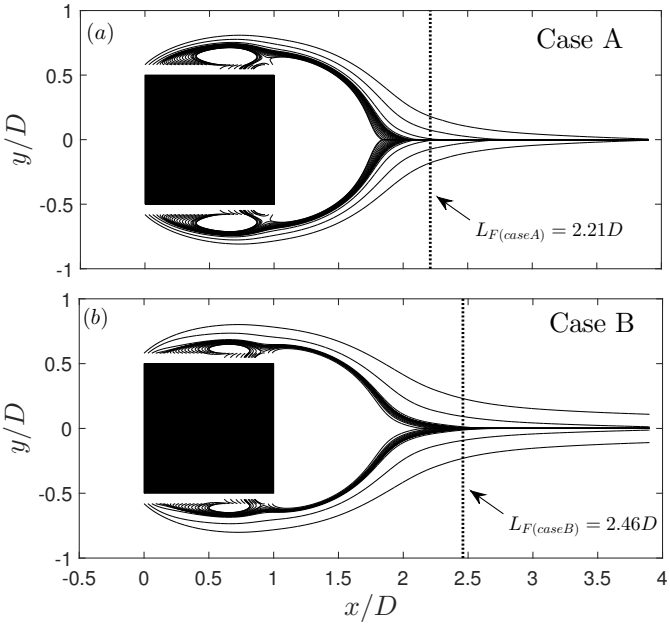

FIG. 10: streamlines highlighting the mean base-region (a) Case A; (b) Case B. Also showing vortex formation-length, L_F, defined as the distance along the wake centreline from the origin on the front face to the location of max $\sqrt{\overline{\tilde{v}\tilde{v}}}/U_\infty$, estimated from Fig. 9 (a).

addressed in the result presented in § V C 2.

Figs. 12 ($a-e$) and ($f-j$) present the normalised phase-averaged coherent cross-stream Reynolds normal stress, $\tilde{v}\tilde{v}^\phi/\overline{U}^2_\infty$ at constant phases $\phi = 0$ to π for Case A and Case B, respectively. The strong region around $(x, y) = (2.36, 0.00)$ is associated with the positive $\tilde{v}$ of the anticlockwise rotation of the lower vortex while the region closer to the body is associated with negative $\tilde{v}$. Similarly, in Fig. 13 (a), regions of concentrated organised streamwise Reynolds stresses, $\tilde{u}\tilde{u}/\overline{U}^2_\infty$, are above and below the vortex core and are associated with the upper and lower shear layers. Both components of Reynolds normal stresses follow the vortex centre as it convects downstream. Comparing Case A and B, the magnitude of $\tilde{v}\tilde{v}/\overline{U}^2_\infty$ in Case B is reduced, particularly on the wake centreline, while in the streamwise direction, $\tilde{u}\tilde{u}/\overline{U}^2_\infty$ appear slightly enhanced in the turbulent case. This is evident across the range of ϕ presented, but is most notable at $\phi = 0$ where the lower VK vortex is still close to the base of the cylinder. These observations agree with the phase-averaged vorticity fields presented in Fig. 11; however, the magnitude differences cannot be accurately inferred from Figs. 11-13 nor can it be distinguished between changes to the levels of random and coherent energy in base and wake section; the following section addresses this point.

3. Coherent & random contributions to global Reynolds stresses in the base & wake regions

Figs. 14 & 15 present profiles of the triple decomposition outlined in § IV A to illuminate changes to the coherent and random components of the fluctuating energy in the wake and base regions of the square cylinder. For both cases, the coherent cross-stream turbulent stresses, $\overline{\tilde{v}\tilde{v}}/\overline{U}^2_\infty$, increase with downstream distance, reach a maximum value and then decrease farther downstream. Focusing where the most dramatic changes were observed in § V B 2, the cross-stream Reynolds stresses along the centreline are observed to reduce substantially with the addition of FST; both the coherent and random are seen to halve, where their respective differences are largest. More specifically, $\overline{\tilde{v}\tilde{v}}/\overline{U}^2_\infty$ are reduced by 50% at $x/D = 1.8$, while the random stresses are reduced by 52% at $x/D = 1.6$ as observed in Fig. 14. Moreover, farther downstream ($x/D > 3.7$), the effect of FST diminishes and the magnitude of the cross-stream Reynolds stresses for both cases is similar.

Considerable differences are also observed in the streamwise turbulent Reynolds stresses, however, these are more pronounced away from the wake centreline. Fig. 15 illustrates the downstream evolution of the streamwise fluctuations in the base and wake regions; the contribution of the coherent fluctuations ($a-c$) starts and finishes with very slight differences, however in the range $2 \leq x/D \leq 2.75$, Case B is up to 40% larger at $\sim y/D = -0.5$. It is interesting that the global r.m.s values presented in Fig. 8 did not reveal these differences; only upon separating the random and coherent parts are the changes apparent.

To summarise this section, it is apparent that FST has the most pronounced effect in the base region ($1 < x/D = 2.5$) where interaction between shear layers is important. The above observations are in and of themselves insightful as they reveal

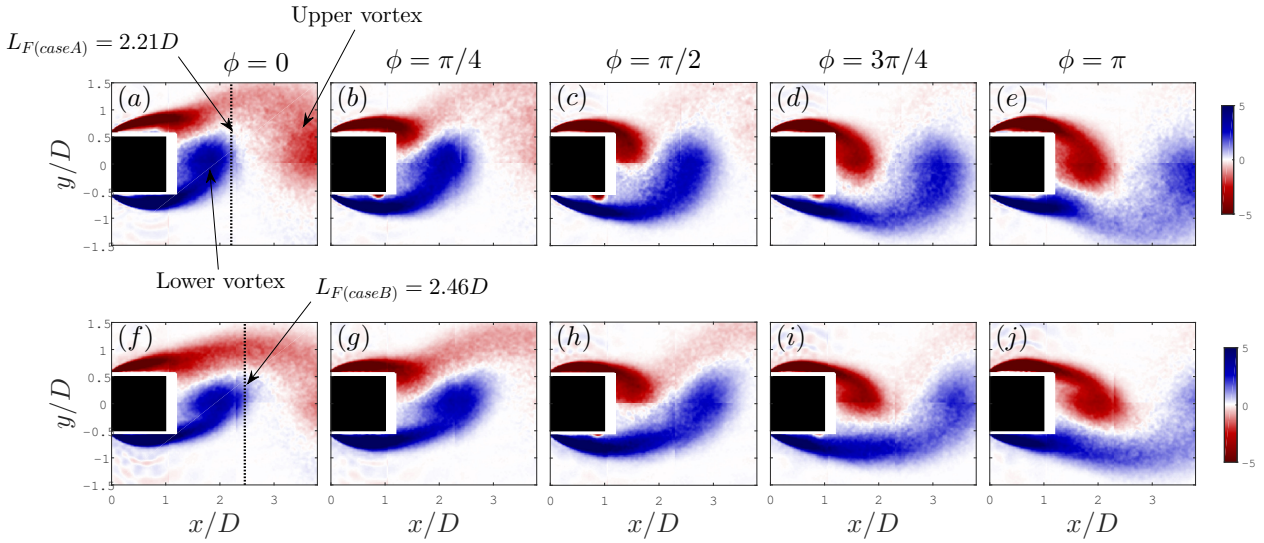

FIG. 11: Phase averaged normalised vorticity $\langle\omega_z\rangle^{\phi} D/\overline{U}_{\infty}$ at five phases along the shedding cycle; $(a-e)$, Case A $(f-j)$, Case B

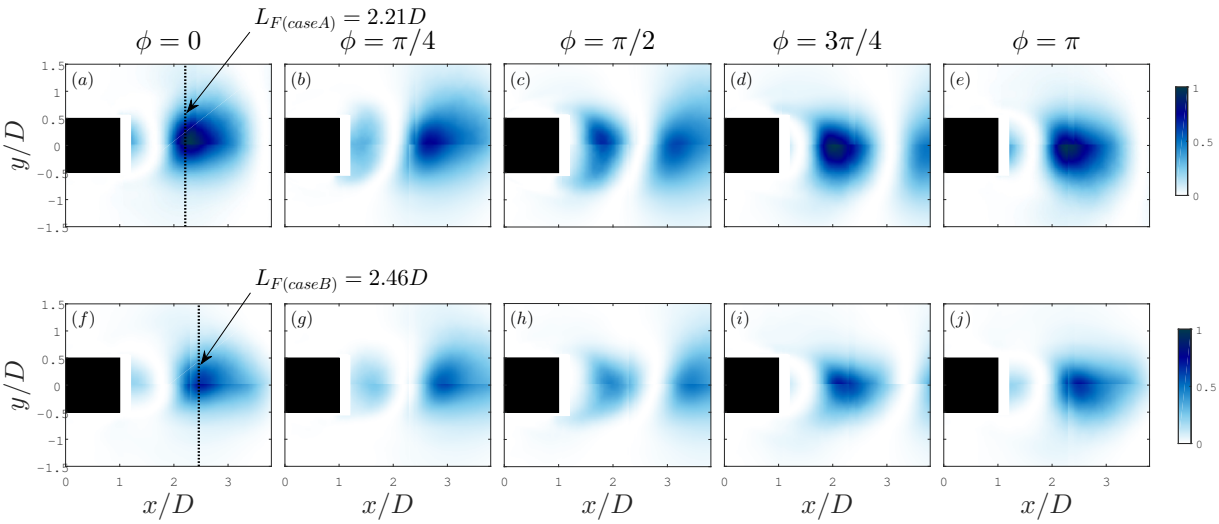

FIG. 12: Phase-averaged normalised coherent cross-stream Reynolds normal stress, $\tilde{v}\tilde{v}^{\phi}/\overline{U}_{\infty}^{2}$ at $\phi = 0$ to π; $(a-e)$: Case A $(f-j)$: Case B

some of the underlying dynamic features of the wake narrowing and elongation, which have been frequently observed in the time-averaged limit of the square cylinder wake. These are the altered dynamics, which accompany the reduced base pressure and consequently the drag force. Furthermore, they show that perturbations along the stagnation streamline are important to the observed changes to the flow field and resulting changes in loading on the body. However, the essential mechanism governing these changes, which must result from instantaneous interaction of the front face boundary layer and shear layer with the FST remain difficult to characterised from the data presented thus far. Further still, it remains to be explained how these disturbances propagate into the wake causing the observed changes to the large scale coherent motions associated with the von-Kármán vortex street. The following section offers some treatment of these outstanding features.

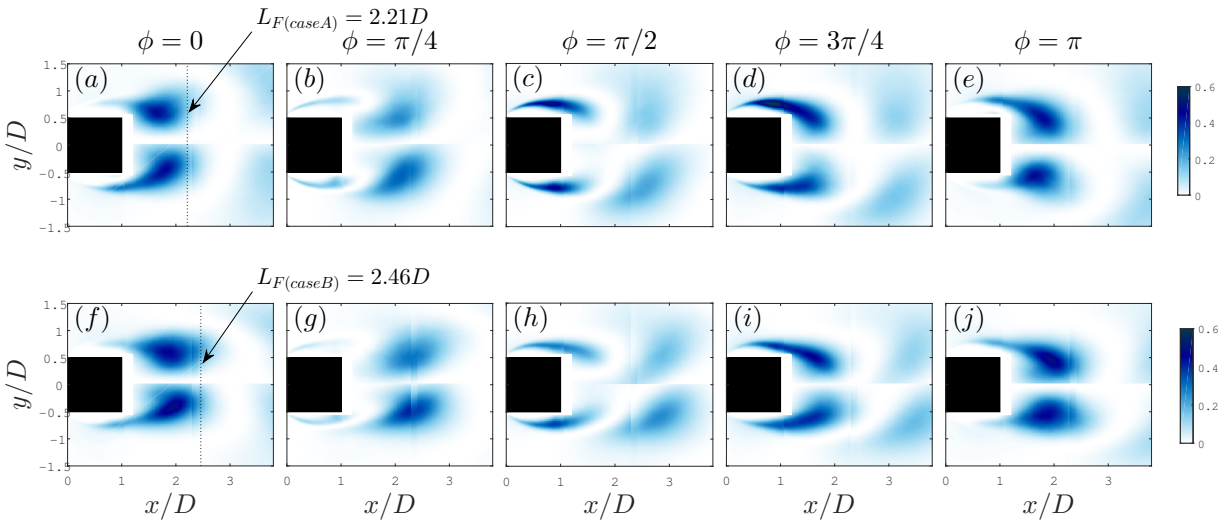

FIG. 13: Phase-averaged normalised coherent streamwise Reynolds normal stress, $\tilde{u}\tilde{u}^{\phi}/\overline{U}_{\infty}^{2}$ at $\phi = 0$ to π; $(a-e)$: Case A; $(f-j)$: Case B

C. The shear layer region

1. *Shear layer region: Mean flow*

Frequently cited as a rationale for the changes in wake characteristics observed in § V B is an intermittently reattaching shear layer [12–14, 46]. Length-scales of FST proportional to the width of the shear layer are said to accelerate the growth rate and curvature toward the wall, which increase the opportunity for reattachment. It was proposed by Gartshore [9] that FST arriving along the stagnation streamline was responsible for the increased growth of the shear layer due to the rapid distortion of turbulent eddies arriving alone this trajectory: "the mean flow field will stretch the vorticity which crosses the stagnation line and which has an initial direction normal to the free stream and the body generators, and will thereby create shear layers shed from the sharp front corners of the body which contain intense, small-scale, stream wise vorticity. ... The shear layers containing the unusual vorticity will thicken more rapidly than would be the case without the initial turbulence." These ideas can be interrogated directly and are presented in Fig. 16. The shear layer curvature is estimated by $y_c = (\mathrm{d}\overline{U}/\mathrm{d}y)_{max}$, the locus of maximum streamwise velocity gradient at each x/D; the shear layer thickness is quantified using the vorticity thickness, defined in Eq. 4 following the work of others [15, 47]. Here, $\Delta\overline{U}_{max}$ is the largest velocity difference across the shear layer while $\mathrm{d}\overline{U}/\mathrm{d}y$ is a measure of the local vorticity concentration at the shear layer centre.

$$\delta_{\omega} = \frac{\Delta\overline{U}_{max}}{\frac{d\overline{U}}{dy}} \tag{4}$$

As can be seen from Fig. 16 (a), the increased curvature of the shear layer is significant as predicted. Data of Lyn & Rodi [48] are also presented and good agreement is seen with the comparable data. Fig. 16 (b) & (c) present the vorticity thickness and the growth of the shear layer $\mathrm{d}\delta_{\omega}/\mathrm{d}x$ with downstream distance is approximately linear for both cases, which is similar to planar mixing layers [49]. For Case A, the results of Lyn *et al.* [48] for a shear layer bounding a turbulent recirculation region and of Castro & Haque [17] on a normal-plate-splitter-plate are also presented. Due to the influence of the recirculation region the growth rate is higher than observed in plane mixing layers [17], although still within the range observed by Brown & Roshko [49] where $0.15 \leq \mathrm{d}\delta_{\omega}/\mathrm{d}x \leq 0.22$.

In Fig. 16, even for Case A, there are quite large differences between studies, which with respect to Castro & Haque [17] it is likely due to the presence of reattachment on the splitter plate at $x/D = 1$. For Lyn *et al.* [48], the observed differences are less pronounced, although in that study the authors reported a step-like behaviour, which they attributed to the periodic presence of the recirculating eddy beneath the shear layer caused by the large scale oscillation of von-Kármán vortex street. While this phenomenon is also present in the current data, the apparent reduction in growth rate in the range $0.5 < x/D < 0.75$ is not observed. Nevertheless, fair agreement is present with that study otherwise. With enhanced FST, as shown in Fig. 16 (c), the results compare well with that of Castro & Haque [17] ($\sqrt{\overline{uu}} = 3.5\%$ & $L_u^x/D \simeq 0.65D$) with the trend of decreasing growth rate being consistent between experiments, i.e. decreasing with increasing x/D.

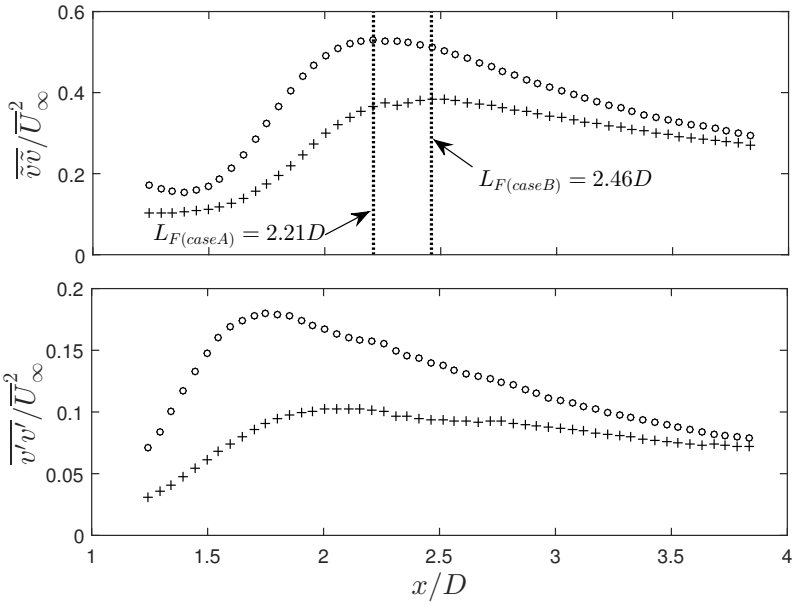

FIG. 14: Streamwise distribution of the cross-stream Reynolds stresses along the wake centreline; (a) coherent, $\overline{\tilde{v}\tilde{v}}/\overline{U}_\infty^2$; ($b$) random, $\overline{v'v'}/\overline{U}_\infty^2$, Case A; +, Case B.

It is interesting to note that the shear layer growth rate is not substantially larger in Case B, as reported elsewhere [15, 17, 50]. However, the mechanisms through which FST affects the growth rate of the shear layer are complex and still not well understood [14]. Certainly, the development of coherent structures in the shear layer via the KH instability during transition plays a roll; subsequent pairing of two or more adjacent spanwise vortices into a single vortex would indeed be accompanied by an abrupt increase in the shear layer width. Note, this would not be identified in the mean growth rate due to the large spatial variation where KH-pairing occurs in unforced mixing layers [51], especially when superimposed on the flapping motion of the VK vortex formation process [48]. If FST affects this process by regularising the KH-pairing process, one would expect an abrupt change in the growth rate similar to those observed in forced mixing layers [52], although this is clearly not visible in the current data. The work by Wygnanski & Petersen [52] is interesting as it demonstrates the decisive control authority on mixing layer growth rates exhibited by periodic disturbances and the opportunities to control the downstream wake formation region. This is of considerable interest to the authors. More recently, the transition process of a circular cylinder shear layer has been considered in the presence of FST [25]. They reported increasing levels of turbulence intensity brought the location where transition occurred closer to the body, for a constant Re_D. In all cases, once transition had occurred, the growth rate was approximately equal between cases and displayed linear growth with $\mathrm{d}\delta_\omega/\mathrm{d}x = 0.15$.

Fig. 17 (a) presents the locus of maximum TKE, defined in Eq. 5.

$$TKE = \frac{1}{2}(\overline{uu} + \overline{vv})/\overline{U}_\infty^2 \tag{5}$$

In the initial stages of development, $0 < x/D \leq 0.2$, Case B has considerably larger TKE; farther downstream, for $x/D > 0.2$, the TKE for both cases increase linearly; however, for Case B it is at a lower rate. Toward the rear of the body, the growth of maximum TKE declines and finally becomes negative as the shear layer approaches the base region. Closer inspection of the constituents of maximum TKE ($\overline{uu}$ and $\overline{vv}$) reveals that the initially larger TKE in Case B is dominated by contributions of $\overline{vv}$, while beyond this point, in both cases, the fluctuations are preferably contributed to by $\overline{uu}$. These trends will be further discussed in the following section. Fig. 17(b) presents the locus of maximum vorticity, and again, in the initial stages of development there are significant differences. At $x/D = 0.1$ the maximum vorticity is 40% smaller in the presence of enhanced FST; however, by $x/D = 0.5$, the difference is negligible.

The increase in maximum TKE and decrease in maximum vorticity, $\overline{\omega}_z$ in the initial stages of development indicates the linear growth region of the shear layer has been altered. In the absence of FST this would form cores of concentrated vorticity associated with the KH instability. Comparing Case A and B, as outlined in § III B, the total circulation generated from the corners is reduced by only 8%. Accordingly, the initial reduction in maximum $\overline{\omega}_z$ must be associated with diffusion, rather than reduced vorticity production. However, quite remarkably, the intensity differences are nullified by $x/D = 0.5$; this suggests that the effect of the enhanced FST introduced along the stagnation streamline on the concentration of vorticity is only to

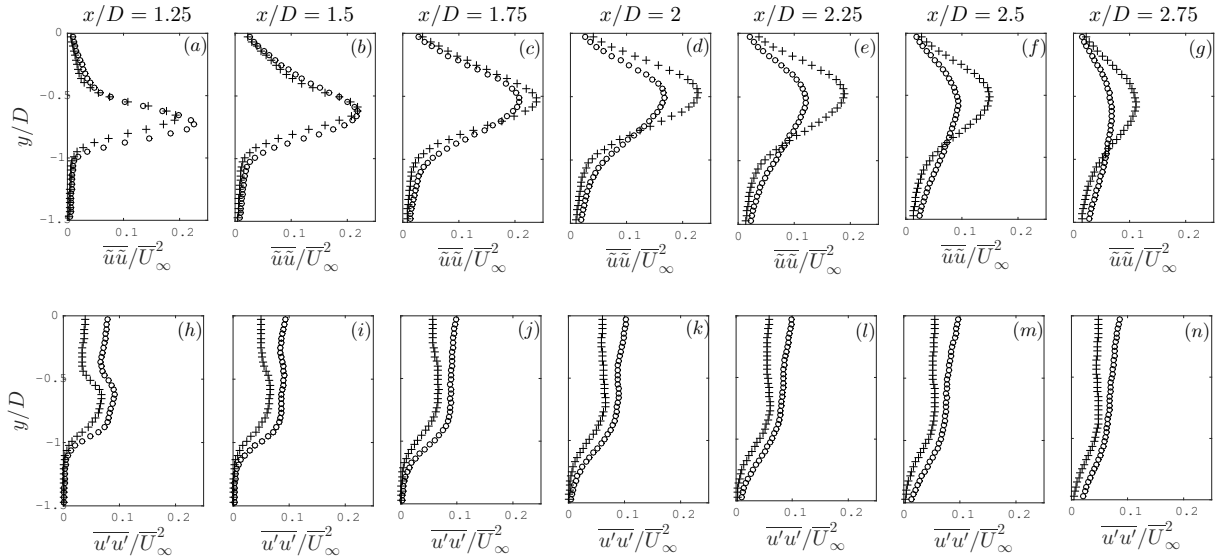

FIG. 15: Cross-stream distribution of the normalised streamwise Reynolds at multiple streamwise locations; $(a-g)$ coherent, $\overline{\tilde{u}\tilde{u}}/\overline{U}^2_\infty$; $(h-n)$ random, $\overline{u'u'}/\overline{U}^2_\infty$. $\circ$, Case A; $+$, Case B.

alter the initial development rather than to cause a sustained increase in the diffusion rate in the shear layers with increasing x/D. It would appear that once Case A has completed the undisturbed transition process, the vorticity concentrations quickly equalise. However, as observed in Fig. 16 (a) this is significant enough to change the overall trajectory of the shear layer to be closer to the body, which will increase the likelihood of reattachment.

2. Instantaneous flow field in the shear layer region

To further investigate the underlying mechanics of these processes, six consecutive instantaneous PIV fields of velocity superimposed over contours of *Q-criterion* in the shear layer region are shown in Fig. 18. The *Q-criterion* is defined as:

$$\boldsymbol{Q} = \frac{1}{2}[|\boldsymbol{\Omega}|^2 - |\boldsymbol{S}|^2] \tag{6}$$

Where $\boldsymbol{S} = \frac{1}{2}[\boldsymbol{\nabla v} + (\boldsymbol{\nabla v})^T]$ is the rate-of-strain tensor and $\boldsymbol{\Omega} = \frac{1}{2}[(\boldsymbol{\nabla v})^T - \boldsymbol{\nabla v}]$ is the rate-of rotation tensor [53]. A vortex is identified as a spatial region where rotation exceeds the rate of strain. Langari & Yang [28] used the *Q-criterion* to identify the KH instability structures in the shear layer of a separation bubble in the presence of FST and found it promising for distinguishing the underlying differences in the instantaneous flows. The sequence presented in Fig. 18 is during the shear layer downswing towards the side wall. Note that between cases, data were taken during separate acquisitions and presented side-by-side only to contrast the instantaneous physical differences between the cases.

In Case A shown in Fig. 18 the typical transition process is clearly observed. In frame (a), KH vortices are present in the separated mixing layer and several vortices are observable within the shear layer region over the length of the body; at $x/D \simeq 0.4$, signs of vortex pairing are evident. In frame (b) a second stage of pairing appears; between frame $(c-e)$, this larger shear layer vortex convects downstream before breaking apart into randomly dispersed cores, signifying complete transition. In contrast, in Case B, Fig. 18 $(g-l)$, the development of the coherent KH vortices are clearly changed. In frame (g), at $x/D \simeq 0.15$, multiple KH vortices have amalgamated. These smaller vortices coalesce into a single larger vortex in frame (h), while moving downstream. By frame (i) the larger vortex has broken apart into randomly dispersed cores in a similar process to Case A but much closer to the separation origin. The randomly dispersed cluster retains a global anti-clockwise circulation and convects more slowly than the individual KH vortices. This entrains freestream fluid on the downstream edge of the cluster, as observed in frame (k). In frame (l), the altered transition process culminates with a blitz of entrained freestream fluid on the side face, trapping the shear layer and causing reattachment.

The process described here is analogous to that observed during bypass-transition [24, 28] of a shear layer bounding a separation bubble on a flat plate. Through the use of DNS simulations, the origins of bypass transition are identified to be associated with development of turbulent spots, which evolve in the presence of large instantaneous streamwise velocity fluctuations forming in the laminar boundary layer upstream of separation. [24] The large favourable pressure gradient on the front face of the square cylinder is likely to resist the formation of streaks and spots in the boundary layer; thus, whether

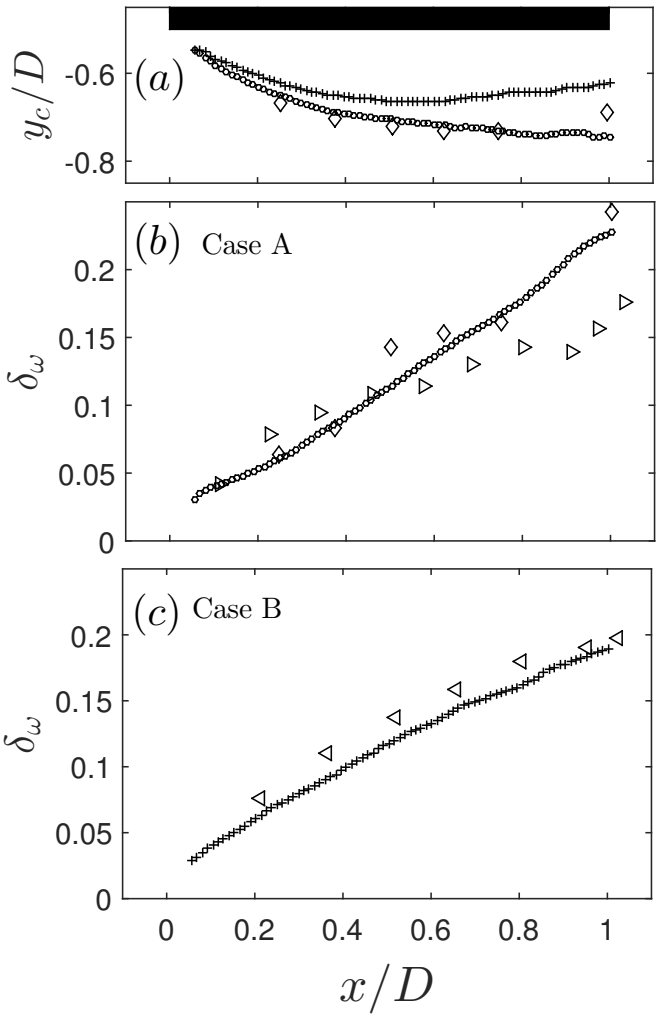

FIG. 16: mean properties of the shear layer: (a) the location of the centre of the shear layer, $y_c = (\mathrm{d}\overline{U}/\mathrm{d}y)_{max}$; ($b$) & ($c$) vorticity thickness, $\delta_\omega = \Delta\overline{U}_{max}/(\mathrm{d}\overline{U}/\mathrm{d}y)_{max}$, Case A and Case B, respectively. ∘, Case A, present; +, Case B, present; ⋄, ambient FST only, Lyn *et al.* [48]; ◁, enhanced FST ($\sqrt{\overline{uu}}/\overline{U}^2_\infty = 3.5\%$ & $L^x_u/D \simeq 0.65D$) , Castro & Haque [17]; ▷, ambient FST ($\sqrt{\overline{uu}}/\overline{U}^2_\infty < 0.25\%$, Castro & Haque [17];

there exists a common origin to the bypass transition observed where the boundary layer develops with small or mild pressure gradients is questionable. This is currently beyond the scope of the current investigation because no measurements were made on the flow approaching the front face of the body. Notwithstanding, similarly to the current results, Langari & Yang [28] found the KH instability was entirely bypassed, leading to earlier breakdown into turbulence, as found here.

The observations of Fig. 18 complement those of Fig. 17 (a); the increased global averaged maximum TKE (specifically, $\overline{vv}$) during the initial stages of shear layer development are associated with the onset of transition closer to the separation. Specifically, the enhanced turbulent cross-stream fluctuations for $0 < x/D < 0.15$ are concomitant with the rapid KH vortex pairing immediately downstream the separation point. The relative reduction in maximum TKE ($\overline{uu}$) for $x/D > 0.2$ is presumably an aftereffect of the accelerated transition process and is likely associated with the relinquished opportunity of vortex pairing and therefore larger intensity streamwise fluctuations. Additionally, the converging of maximum vorticity intensity observed in Fig. 17 (b) at $x/D \simeq 0.5$ can now be seen to follow closely the first stage of KH vortex pairing in Case A, a process which is observed to quickly form large vortices before disbanding into smaller randomly distributed cores. Clearly, the high values of maximum normalised vorticity for $0 < x/D < 0.15$ are associated with the highly concentrated and coherent line of KH cores, a feature absent in the presence of enhanced FST. Further still, the increased curvature of the shear layer in the presence FST can also be explained: the early pairing of KH vortices into clusters keeps the shear layer initially closer to the body while the associated freestream fluid entrained between clusters draws the locus of maximum shear closer to the body.

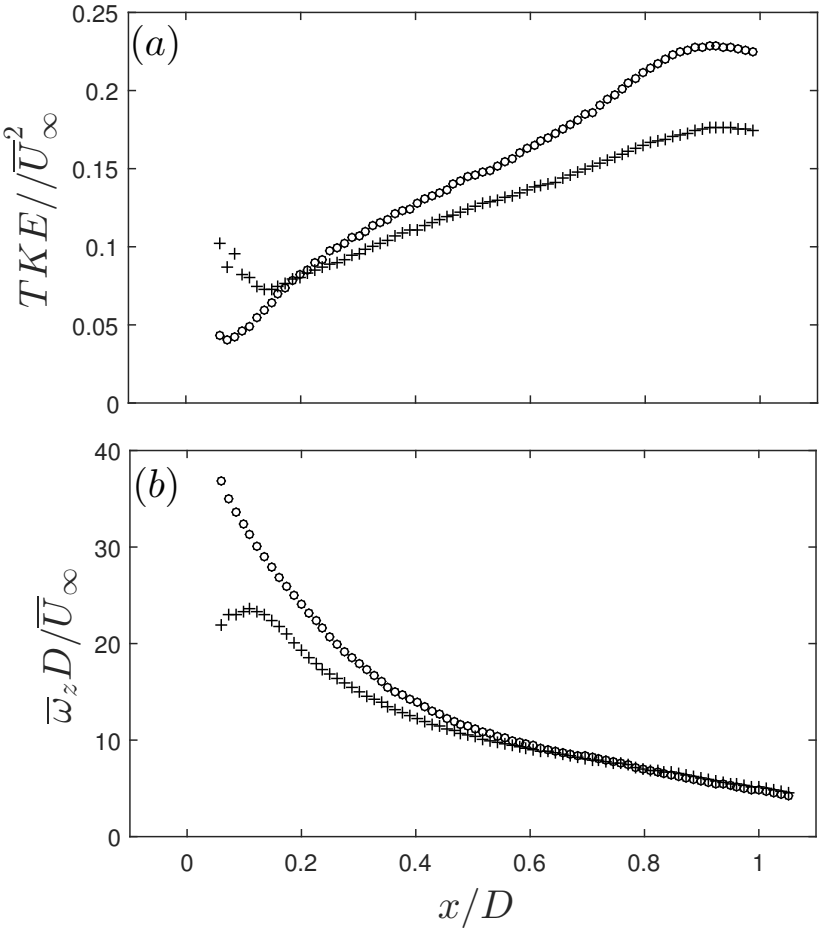

FIG. 17: (a) locus of maximum TKE in the shear layer region and (b) locus of maximum vorticity in the shear layer region; ∘, Case A; +, Case B.

3. Shear layer entrainment & the diffusion length

Fig. 19 presents the phase averaged normalised vorticity of the lower shear layer in the base region at $\phi = 0$. The bounds of the shear layer are taken as the spatial extent where $\overline{\omega}_z^\phi D/\overline{U}_\infty > 1.1$. This value represents the spatial extent of the shear layer where the vorticity is larger than 10% of the maximum at $x/D = 0.5$, which, as observed in Fig. 17 (b), is where the locus or maximum vorticity converges between the two cases. In § V C 2, this was identified as the location where shear layer transition in Case A was close to completion. It is observed in Fig. 19 that the streamwise extent of the shear layer is very well aligned with the formation length in both cases, which, as described by Bloor, [45] indicates the start of a new cycle and is accompanied by irrotational flow crossing the wake centreline, or as previously denoted, L_F. Thus this definition to describe the spatial boundary of the shear layer is agreeable with other wake descriptions and will serve to discuss apparent differences between cases.

In Fig. 19 (a) & (b), the markers indicate the locus of max vorticity, similarly to that presented in Fig. 17 (a). The locus is continued into the base region marking a continuous trajectory between separation and the forming vortex. In frame (c) the magnitude of the shear layer's vorticity along the trajectories is presented; similar to Fig. 17 (b), the maximum $\overline{\omega}_z^\phi D/\overline{U}_\infty$ is lower in Case B only in the range $0 < x/D < 0.2$. As can be seen, the maximum vorticity along the shear layer remains almost identical all the way into the base-region despite traversing substantially different paths. If the maximum vorticity along these loci are a measure of the rate of vorticity diffusion, it indicates that the enhanced FST did not cause substantially increased exchange through the shear layer. Alternatively, the FST has not substantially increased the entrainment rate of irrotational flow into the shear layer, which would be marked by a spreading of vorticity and a reduction of the magnitude along the loci. Furthermore, recalling there are only slight differences in rate of circulation generated between cases, it is apparent that the observed changes to the aerodynamic parameters are caused by the bypass-transition behaviour and the subsequent interaction with the body rather than via a substantial change in the turbulent mixing rates.

The differences between cases observed in Fig. 19 (a) & (b) are complementary to those observed in Figs 14 & 15 where cross-

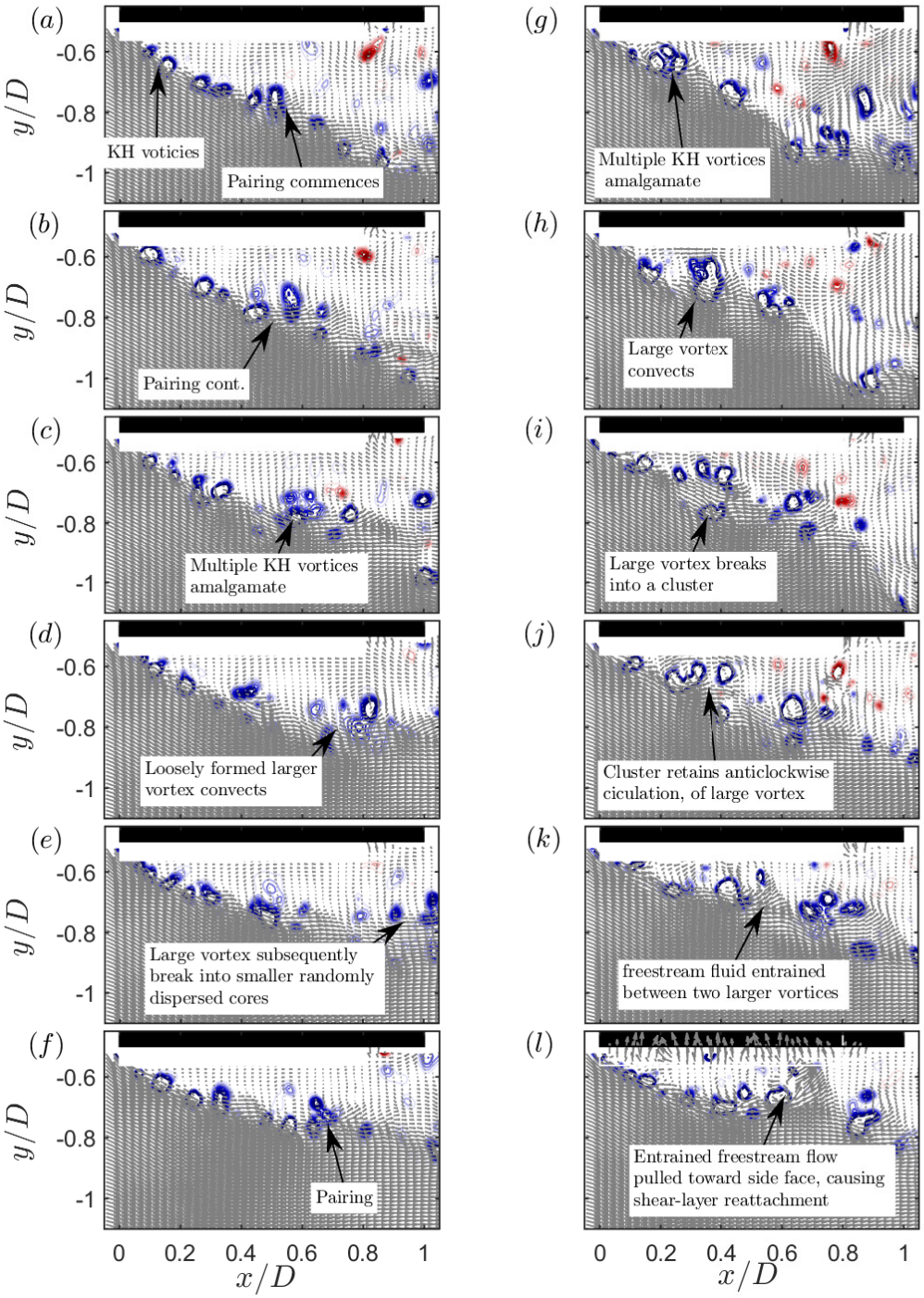

FIG. 18: Comparison of the instantaneous in-plane velocity vectors superimposed with contours of instantaneous *Q-criterion* for the shear layer during the downswing to its minimum position; Case A, $(a - f)$; Case B, $(g - l)$

stream shear layer wake stresses were reduced in favour of the streamwise components. In Fig. 19 (a) & (b), the relationship to the shear layer development is apparent: in Case B, the shear layer trajectory moves toward the lee of the body and the forming VK vortex is clearly elongated in the streamwise direction while its reach across the wake centreline is limited. This is a consequence of the intermittent reattachment which occurs on the leeward edge, which in the phase-averaged data is shown by a clear region of "necking" as the shear layer straightens in the streamwise direction following its interaction with the body.

Here, it is worthwhile to consider the work of Gerrard [30] whose phenomenological model of vortex shedding required the diffusion length, L_D, in addition to the formation length, L_F, to account for the constancy of St in the presence of changing Re of the circular cylinder in the subcritical range. The opposing tendencies of L_F and L_D are thought to act via the same mechanism, namely, the intensity of the turbulence stresses in the shear layer, which affects the balance of entrainment rates into the shear layer and forming vortex. Gerrard suggested that increasing the FST should increase the entrainment and increase L_D, which in the case of the circular cylinder would be accompanied by a reduction in L_F. The opposing changes balance to keep St_D constant in the presence of reduced wake size, which, in a thin shear layer model [6], would be accompanied by smaller vortices and increased shedding frequency.

The constancy of St_D is also observed for the square cylinder over a large range of Re_D where comparable shear layer transition processes are present in the subcritical range [54]. Accordingly, Gerrard's model should retain relevance to the square cylinder, as well as other geometries. Taylor *et al.* [55] discussed the need to focus on the characteristics of the diffusion length as a parameter to assist a sensible universal St_D while studying the flow around elongated bluff bodies. In these cases, the presence of an afterbody increases rather than decreases L_F via the reattachment mechanism, and in the present study, L_F increases by $\sim 11\%$. Using Gerrard's rationale it can be hypothesised that as the formation length increases, the diffusion length must decrease to keep St constant; however, recall that St_D increased with the addition of FST (see: Fig. 5(d) where $1.05 \times St_{(CaseA)} \simeq St_{(CaseB)}$). Defining the L_D as the Euclidean distance of the vector $\boldsymbol{AB}$ illustrated in Fig. 19 (a) & (b), which is that perpendicular to the shear layer centre as it crosses the wake centreline at phase $\phi = 0$, the diffusion length can be written as $L_D = \|\vec{\boldsymbol{AB}}\|$. Here, $L_{D(CaseA)} = 0.89D$ and $L_{D(CaseB)} = 0.86D$, or a 3.5% decrease. This is the correct trend of L_D, and indeed, it almost balances the change in L_F when the increase in St_D is considered. However, the utility of this measure requires investigations across a broader range of FST intensities or over a wider range of Re_D to substantiate this approach to the definition of L_D.

VI. DISCUSSION

It remains to comment on the connection between changes observed in the shear layer region to those observed in the wake and connection to the global aerodynamic features such as L_F and C_{pb}. In § V A, it was reported that the drag coefficient, C_D, reduced by 21%, from 2.35 to 1.86; 12% of the total reduction was attributable directly to the altered wake dynamics. Careful consideration of the shear layer revealed that an accelerated transition processes considerably alters the trajectory of the mean and phase averaged shear layer without causing increased vorticity diffusion from the shear layer into the base, as indicated by the loci of maximum vorticity. As a consequence, the VK vortex forms farther from the body. Bearman & Trueman [46] discussed the streamwise distance from the body where the VK vortex forms; larger distances are directly correlated to a rise in base pressure and therefore reduced drag. This relation is exemplified by the rapid increase and precipitous decrease in base pressure when the transverse to streamwise dimensions of the body approaches and passes $B/D = 0.62$. This remarkable change occurs in the presence of unchanged total circulation (i.e., without changing the freestream velocity) entering the wake during a period of VK shedding; the increase as B/D approaches 0.62 is a consequence of the space occupied by the afterbody in the base region while the formation length is unable to increase. This reduces C_{pb} further below the static pressure and increases the vorticity generation. As B/D passes 0.62, the body has a more pronounced influence and starts to increase the formation length, which then brings C_{pb} back toward the pressure in the freestream. This geometric influence of afterbody helps explain the substantial consequence on the global aerodynamic parameters like C_{pb} due to relatively small changes to the shear layer transition process; i.e. the new trajectory of the shear layer closer to the body is synonymous with an increase in the length of the body. This is not a new analogy to explain the effects of small scale FST [12], however, identifying the mechanism as a bypass transition occurring in the shear layer appears to be previously unreported. It should be noted that this would also result in a decrease in unsteady lift as the individual vortices are less imposing when forming farther downstream [43].

A comment on the ideas presented by Gartshore [9] would be valuable at this point. The author proposed and observed that FST introduced along the stagnation streamline was responsible for the most distinct changes to $2D$ bluff body flows. Ostensibly, the effects of grid generated small-scale FST were able to be replicated with only that arriving on or close to the stagnation streamline; results which have largely been confirmed here. Central to his thesis was that small-scale eddy structures on this approach trajectory are distorted and amplified by the blockage of the body and the strain field of the mean flow as it is retarded by the presence of the body. This intuition calls on theory of Batchelor & Proudman [56] and Hunt [57] and experiments of Bearman [46]. Rapid distortion of the stagnation streamline FST increases the availability of streamwise vorticity, which when in proximity to the shear layers causes more rapid growth, entrainment and consequently, curvature. Interestingly, the theoretical and numeric work of Meliga *et al.* [58] found a region of high drag sensitivity exists along the stagnation streamline when using a small circular cylinder to impose a disturbance on the flow field. Its presence had decreasing influence as it was moved in either cross-stream direction off the stagnation line, which corroborates the present findings and those of Gartshore [9]. The present study provides some points which help uncover the underlying phenomenological details which ought to be considered; as measured by the vorticity thickness, δ_ω, neither a substantially higher growth rate nor a substantially increased rate of vorticity diffusion by the shear layers was observed. However, a considerably altered transition

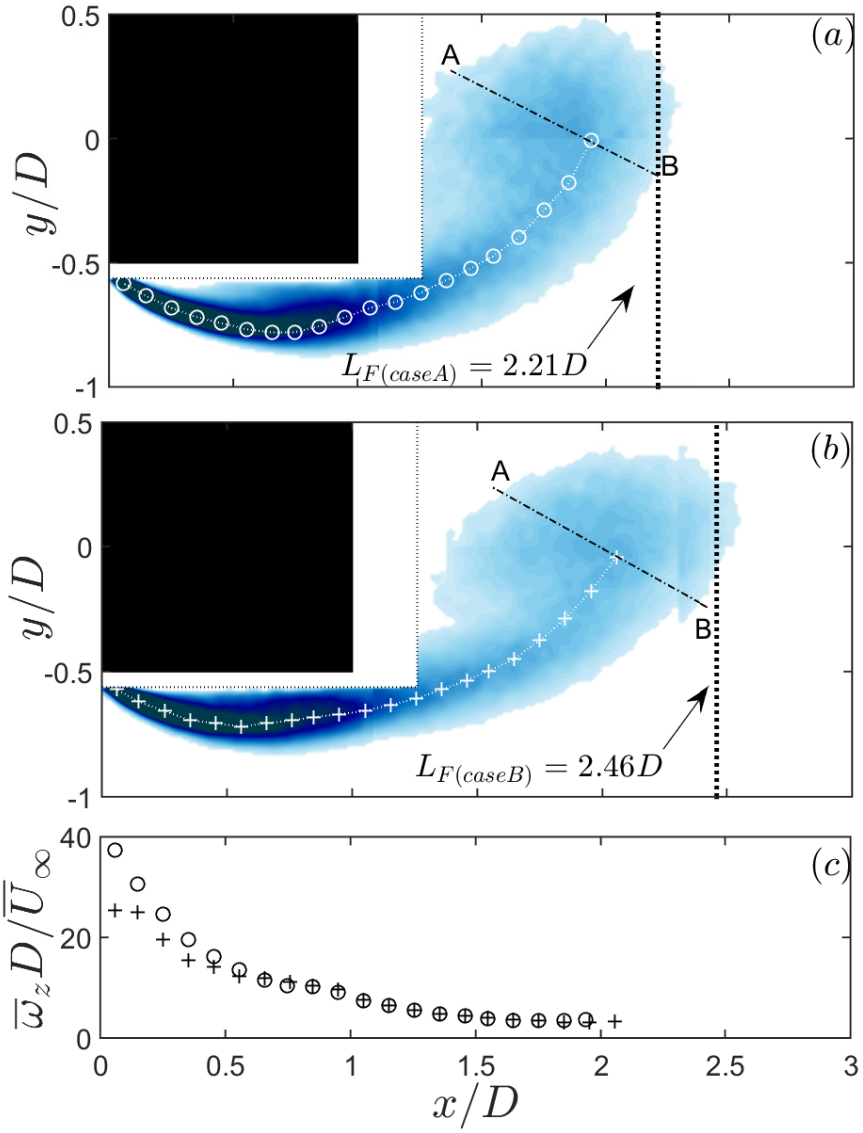

FIG. 19: Normalised phase averaged vorticity, $\overline{\omega}_z^\phi D/\overline{U}_\infty$, of the shear layer in the base region at $\phi = 0$. White markers indicate approximate positions of max vorticity emanating from the separation origin. (a) Case A and (b) Case B; (c) magnitude of vorticity along the shear layer centrelines above ∘, Case A; +, Case B

process, analogous to that observed during bypass-transition of boundary layers was observed. This was responsible for the observed mean shear layer position tending closer to the body. It should be noted that Gartshore did not suspect an altered transition process: "...the addition of free stream turbulence, if it simply promotes early transition in the shear layers, is unlikely to alter the flow pattern significantly if the value of Re is above 3×10^4". Conversely, as reported in § V C 2 via the observations of the instantaneous shear layer development, the FST is seen to interact with the KH vortices immediately following separation causing them to cluster into groups and the reattachment-type response that ensued as a consequence of this amalgamation has been discussed at length herein. It seems quite plausible that this was the phenomenon that Gartshore encountered. Unfortunately, it is not possible with the current data to confirm the presence of additional streamwise vorticity entering the front face boundary layers nor evaluate its effect on the growth rate of the shear layers. Nonetheless, the concept

of shear-sheltering [59, 60] has since provided evidence that the penetration depth, δ_p, of freestream disturbances into a boundary layer are both frequency and Reynolds number dependent according to $\delta_p \propto (\omega Re)^{-0.13}$ (here, $\omega = 2\pi/f$ is the angular frequency); i.e. the time-mean shear of the viscous laminar boundary layer filters high frequency disturbances. The range of disturbance frequencies which penetrate deepest into the boundary layer is dependent on the experimental parameters $\sqrt{\overline{uu}}/\overline{U}_\infty$ and L_u^x/D; however, the fluctuations that do penetrate are expected to be lower than the integral scale and much lower than those which would be amplified by the Tollmien-Schlichting boundary layer instability [24]. Accordingly, the ability of disturbances of the order of the boundary layer thickness to penetrate the front face boundary layer under strong favourable pressure gradient appears to be questionable. Notwithstanding, as observed in the instantaneous *Q-Criterion* fields, the FST evidently may penetrate the shear layer and interact with the vortical structures shortly after separation.

Finally, the present results, while primarily of a fundamental nature, also provide a stark insight into a flow control application. Clearly, the initial stages of shear layer development and the normal pathway to turbulence are fundamentally important to the formation of large scale vortical structures, which are of course responsible for the global forces on the bluff body. It may be possible to exploit this mechanism as a vehicle to ameliorate the unwanted loads on square bluff bodies, a problem which has received considerable attention in the flow control community in recent years [61].

VII. CONCLUSION

Flow with ambient levels and enhanced levels of FST have been studied around a $2D$ square cylinder with an emphasis on understanding the contribution of the shear layer development to altered global aerodynamic characteristics such as drag, base pressure and wake formation length. To isolate the effects of the enhanced FST on the shear layer, a turbulence generating 'rod' upstream of the stagnation streamline was employed. Consistent with other studies, the PIV data indicated a narrowing and lengthening of the wake; this was accompanied by a rise in base pressure, a reduction in mean drag lengthening of the wake formation length. Using triple decomposition, the underpinning dynamics of the wake revealed a streamwise lengthening of the individual von-Kármán vortex structures, complementary to the changes observed to the mean wake. Closer inspection of the shear layer region indicated a substantial increase in curvature towards the body but no pronounced increase in the shear layer growth rate. The loci of maximum TKE and normalised vorticity, $\overline{\omega}_z D/\overline{U}_\infty$, revealed the largest changes occurred in the very initial stages of shear layer development shortly following separation. Inspection of a series of instantaneous PIV fields of *Q-Criterion* showed that the typical transition pathway, via the formation and subsequent pairing of the KH vortices was bypassed. The KH vortices were observed to cluster and amalgamate after separation before breaking into smaller randomly dispersed cores. The bypass transition was observed to be followed by shear layer reattachment in some cases. This was considered the primary mechanism for the reported changes to the large scale aerodynamic characteristics and the altered wake dynamics. Furthermore, a quantitative definition of the "diffusion length" introduced by Gerrard [30] to the square cylinder wake was reported and its relation with the Strouhal number and wake formation length was considered.

ACKNOWLEDGMENTS

The authors wish to express our gratitude to Mr. Abul Fahad Akon and Mr. Gerry Dafoe of the University of Western Ontario and of Mr. Andrew Searle of IO Industries who played an indispensable role during the experimental campaign. To Dr. Cummings for the stimulating conversations and to Mr. Joesph Baker, Mr. Robert Whiting and Mr. Jordan Fisher for their persistence and dedication as undergraduate researchers. Financial support provided by the National Science Foundation under grant NSF CMMI-1200987.

[1] A. Fage and J. Warsap, *Her Majesty's Stationery Office*, Tech. Rep. (London, 1929).
[2] G. B. Schubauer and H. L. Dryden, *The effect of turbulence on the drag of flat plates*, Tech. Rep. 546 (National Advisory Committee for Aeronautics, 1935).
[3] Frederick H. Abernathy and Richard E. Kronauer, "The formation of vortex streets," Journal of Fluid Mechanics **13**, 1 (1962).
[4] Anatol Roshko, "On the Wake and Drag of Bluff Bodies," Journal of the Aeronautical Sciences (Institute of the Aeronautical Sciences) **22**, 124–132 (1955).
[5] C H K Williamson, "Vortex dynamics in the cylinder wake," Annu. Rev. Fluid Mech. **28**, 477–539 (1996).
[6] Anatol Roshko, "Perspectives on Bluff Body Aerodynamics," Journal of Wind Engineering and Industrial Aerodynamics **49**, 79–100 (1993).
[7] C. K. Chyu and D. Rockwell, "Near-wake structure of an oscillating cylinder: effect of controlled shear-layer vortices," Journal of Fluid Mechanics **322**, 21 (1996).
[8] J. H. Gerrard, "A disturbance-sensitive Reynolds number range of the flow past a circular cylinder," Journal of Fluid Mechanics **22**, 187 (1965).
[9] I. S. Gartshore, *BLWTL report-4-73 UWO*, Tech. Rep. (BLWTL, UWO, London, Canada, 1973).

[10] A Laneville, Is Gartshore, and Gv Parkinson, "An explanation of some effects of turbulence on bluff bodies," in *Proceedings of the 4th International Conference on Wind Effects on Buildings and Structures*, edited by K. J. Eaton. (Cambridge University Press, London, 1975).

[11] Wh Melbourne, "Turbulence, bluff body aerodynamics and wind engineering," in *Australiasian Conference on Hydraulics and Fluid Mechanics* (Institution of Engineers, Australia, Barton, A.C.T, 1980) pp. 18–22.

[12] Y. Nakamura, "Bluff-body aerodynamics and turbulence," Journal of Wind Engineering and Industrial Aerodynamics **49**, 65–78 (1993).

[13] Yasuharu Nakamura and Yuji Ohya, "The effects of turbulence on the mean flow past two-dimensional rectangular cylinders," Journal of Fluid Mechanics **149**, 255 (1984).

[14] P.W. Bearman and T. Morel, "Effect of free stream turbulence on the flow around bluff bodies," Progress in Aerospace Sciences **20**, 97–123 (1983).

[15] N. K. Pui and I. S. Gartshore, "Measurements of the growth rate and structure in plane turbulent mixing layers," Journal of Fluid Mechanics **91**, 111 (1979).

[16] M Kiya and K Sasaki, "Free-stream turbulence effects on a separation bubble," Journal of Wind Engineering and Industrial Aerodynamics **14**, 375–386 (1983).

[17] I. P. Castro and A. Haque, "The structure of a shear layer bounding a separation region. Part 2. Effects of free-stream turbulence," Journal of Fluid Mechanics **192**, 577 (1988).

[18] M. F. Unal and D. Rockwell, "The role of shear layer stability in vortex shedding from cylinders," Physics of Fluids **27**, 2598 (1984).

[19] R. Hillier and N.J. Cherry, "The effects of stream turbulence on separation bubbles," Journal of Wind Engineering and Industrial Aerodynamics **8**, 49–58 (1981).

[20] Laurent Perret, "PIV investigation of the shear layer vortices in the near wake of a circular cylinder," Experiments in Fluids **47**, 789–800 (2009).

[21] C. Brun, S. Aubrun, Thomas Goossens, and Ph Ravier, "Coherent structures and their frequency signature in the separated shear layer on the sides of a square cylinder," Flow, Turbulence and Combustion **81**, 97–114 (2008).

[22] M. F. Unal and D. Rockwell, "On vortex formation from a cylinder. Part 1. The initial instability," Journal of Fluid Mechanics **190**, 491 (1988).

[23] Anil Prasad and Charles H. K. Williamson, "The instability of the shear layer separating from a bluff body," Journal of Fluid Mechanics **333**, 375–402 (1997).

[24] Brian R. McAuliffe and Metin I. Yaras, "Transition Mechanisms in Separation Bubbles Under Low- and Elevated-Freestream Turbulence," Journal of Turbomachinery **132**, 1–10 (2010).

[25] Imed Khabbouchi, Hachimi Fellouah, Mohsen Ferchichi, and Mohamed Sadok Guellouz, "Effects of free-stream turbulence and Reynolds number on the separated shear layer from a circular cylinder," Journal of Wind Engineering and Industrial Aerodynamics **135**, 46–56 (2014).

[26] Dan S. Henningson, Anders Lundbladh, and Arne V. Johansson, "A mechanism for bypass transition from localized disturbances in wall-bounded shear flows," Journal of Fluid Mechanics **250**, 169–207 (1993).

[27] P Andersson, M Berggren, and D S Henningson, "Optimal disturbances and bypass transition in boundary layers," Physics of Fluids **11**, 134 (1999).

[28] Mostafa Langari and Zhiyin Yang, "Numerical study of the primary instability in a separated boundary layer transition under elevated free-stream turbulence," Physics of Fluids **25**, 074106 (2013).

[29] L. W. Sigurdson, "The structure and control of a turbulent reattaching flow," Journal of Fluid Mechanics **298**, 139 (1995).

[30] J. H. Gerrard, "The mechanics of the formation region of vortices behind bluff bodies," Journal of Fluid Mechanics **25**, 401 (1966).

[31] C Norberg, "Interaction Between Freestream Turbulence and vortex shedding for a single tube in cross-flow," Journal of Wind Engineering and Industrial Aerodynamics **23**, 501–514 (1986).

[32] E. C. Maskell, *Her Majesty's Stationery Office*, Tech. Rep. (Ministry of Aviation, London, 1965).

[33] Anatol Roshko, *NACA Report 1191*, Tech. Rep. (National Advisory Committee for Aeronautics, 1954).

[34] J. Hinze, *Turbulence*, 2nd ed. (McGraw-Hill College, 1972).

[35] Zachary J. Taylor, Roi Gurka, Gregory A. Kopp, and Alex Liberzon, "Long-Duration Time-Resolved PIV to Study Unsteady Aerodynamics," IEEE Transactions on Instrumentation and Measurement **59**, 3262–3269 (2010).

[36] A. K. M. F. Hussain and W. C. Reynolds, "The mechanics of an organized wave in turbulent shear flow. Part 2. Experimental results," Journal of Fluid Mechanics **54**, 241 (1972).

[37] Brian Cantwell and Donald Coles, "An experimental study of entrainment and transport in the turbulent near wake of a circular cylinder," Journal of Fluid Mechanics **136**, 321 (1983).

[38] P. W. Bearman and E. D. Obasaju, "An experimental study of pressure fluctuations on fixed and oscillating square-section cylinders," Journal of Fluid Mechanics **119**, 297 (1982).

[39] B. E. Lee, "The effect of turbulence on the surface pressure field of a square prism," Journal of Fluid Mechanics **69**, 263 (1975).

[40] S. Szepessy and P. W. Bearman, "Aspect ratio and end plate effects on vortex shedding from a circular cylinder," Journal of Fluid Mechanics **234**, 191 (1992).

[41] Barry Vickery, "Fluctuating lift and drag on a long cylinder of square n a turbulent stream cross-section in a smooth and in a turbulent stream," Journal of Fluid Mechanics **25**, 481—-494 (1966).

[42] DG Petty, "The effec of turbulence intensity and scale on the flow past square prisms," Journal of Wind Engineering and Industrial Aerodynamics **4**, 247–252 (1979).

[43] I. S. Gartshore, "Some Effects of Upstream Turbulence on the Unsteady Lift Forces Imposed on Prismatic Two Dimensional Bodies," Journal of Fluids Engineering **106**, 418–424 (1984).
[44] D. A. Lyn, S. Einav, W. Rodi, and J. H. Park, "A laser-Doppler velocimetry study of ensemble-averaged characteristics of the turbulent near wake of a square cylinder," Journal of Fluid Mechanics **304**, 285 (1995).
[45] M Susan Bloor and J H Gerrard, "Measurements on Turbulent Vortices in a Cylinder Wake," Proceedings of the Royal Society of London. Series A, Mathematical and Physical Sciences **294**, 319–342 (1966).
[46] P. W. Bearman, "Some measurements of the distortion of turbulence approaching a two-dimensional bluff body," Journal of Fluid Mechanics **53**, 451 (1972).
[47] I. P. Castro and A. Haque, "The structure of a turbulent shear layer bounding a separation region," Journal of Fluid Mechanics **179**, 439 (1987).
[48] D. A. Lyn and W. Rodi, "The flapping shear layer formed by flow separation from the forward corner of a square cylinder," Journal of Fluid Mechanics **267**, 353 (1994).
[49] Garry L. Brown and Anatol Roshko, "On density effects and large structure in turbulent mixing layers," Journal of Fluid Mechanics **64**, 775 (1974).
[50] Rajni. P Patel, "Effects of stream turbulence on free shear flows," Aeronautical Quarterly **29**, 33–43 (1978).
[51] Jie Zhi Wu, Hui Yang Ma, and Ming De Zhou, *Vorticity and Vortex Dynamics* (Springer Science & Business Media, 2006) pp. 1–776.
[52] Israel J. Wygnanski and Robert A. Petersen, "Coherent motion in excited free shear flows," AIAA Journal **25**, 201–213 (1987).
[53] J C R Hunt, A Wray, and P Moin, "Eddies, streams, and convergence zones in turbulent flows," in *Center for Turbulence Research, Proceedings of the Summer Program* (1988) pp. 193–208.
[54] Atsushi Okajima, "Strouhal numbers of rectangular cylinders," Journal of Fluid Mechanics **123**, 379 (1982).
[55] Zachary J. Taylor, Roi Gurka, and Gregory A. Kopp, "Effects of leading edge geometry on the vortex shedding frequency of an elongated bluff body at high Reynolds numbers," Journal of Wind Engineering and Industrial Aerodynamics **128**, 66–75 (2014).
[56] G. K. Batchelor and Ian Proudman, "The Effect of Rapid Distortion of a Fluid in Turbulent Motion," The Quarterly Journal of Mechanics and Applied Mathematics **7**, 83–103 (1954).
[57] J. C. R. Hunt, "A theory of turbulent flow round two-dimensional bluff bodies," Journal of Fluid Mechanics **61**, 625 (1973).
[58] P. Meliga, E. Boujo, G. Pujals, and F. Gallaire, "Sensitivity of aerodynamic forces in laminar and turbulent flow past a square cylinder," Phys. Fluids **26**, 104101 (2014).
[59] Robert G Jacobs and Paul A Durbin, "Shear sheltering and the continuous spectrum of the Orr- Sommerfeld equation," Physics of Fluids **10**, 2006–2011 (1998).
[60] J. C R Hunt and P. a. Durbin, "Perturbed vortical layers and shear sheltering," Fluid Dynamics Research **24**, 375–404 (1999).
[61] David Menicovich, Daniel Chapman Lander, Jason Vollen, Michael Amitay, Chris W. Letchford, and Anna Dyson, "Improving aerodynamic performance of tall buildings using Fluid based Aerodynamic Modification," Journal of Wind Engineering and Industrial Aerodynamics **133**, 263–273 (2014).